

POLITECNICO DI TORINO

Master's Degree in Biomedical Engineering



Master's Degree Thesis

In-body localization and tracking for wireless capsule endoscopy using received signal strength of an RF-transmitter

Supervisors

Dr. Paolo MOTTO ROS

Prof. Dr. Ir. Emmeric TANGHE

Ir. Tom VAN DE STEENE

Candidate

Elisabetta DALMAZZO

October 2023

Summary

In this master dissertation, the localization of the wireless capsule endoscopy (WCE) is studied in order to minimize the error. In particular, the influence of the different tissues of which the human body is composed and their impact on localization were analyzed.

To determine the behavior of the WCE a computational model of the gastrointestinal (GI) tract and the WCE have been implemented. Moreover, a finite difference time domain solver simulation on Sim4Life has been used to study how the WCE moves through the GI tract. Four different simulations were considered, three homogeneous and one heterogeneous: one with the air model, one with fat, one with muscle, and one with a complete human body model containing all tissues.

Various parameters were obtained such as the electric field along the entire GI tract, the distance between the transmitter (Tx) and the receiver (Rx), and the behavior of the Tx in the different tissues. Through the analysis of the data obtained it was possible to interpolate them according to a hyperbola and subsequently evaluate the localization error.

It was clear that the position of the WCE along the GI tract influences the results obtained for the homogeneous muscle model and for the Duke heterogeneous model. For the other two models considered, the homogeneous model of fat and air, this parameter does not significantly affect the results obtained. Furthermore, the position of the receivers in respect to the skin in some cases played a key role in the accuracy of the data obtained. Moreover, the only hyperbolic relationship found between the electric field and the distance between the Tx and Rx was the one for the homogeneous air model. The other simulations did not yield this result. Finally, the localization error for the heterogeneous model was the largest one obtained (between 30 and 40 cm), although comparable with the homogeneous one for muscle. The values obtained for fat and air are smaller.

Keywords: wireless capsule endoscopy, localization, computational modeling, different tissues

Acknowledgements

“To those who believed in me even when I couldn’t do it for myself, also from up there”

First of all, I would like to thank Professor Emmeric Tanghe for letting me have the opportunity to work within his group of research. During the time I spent alongside You, I always felt guided and appreciated so thank you very much.

A special thanks go to Tom Van De Steene which followed me side by side along the path of the redaction of this thesis. Thank you especially for your patience, your kindness and your knowledge. Working with you was really inspiring for me and for my future.

Finally, I sincerely thank Professor Paolo Motto Ros whose care in the realisation of this thesis project was indispensable.

Grazie innanzitutto alla mia mamma, mia bilancia nella vita e nelle scelte che essa comporta. Grazie per essere il perfetto equilibrio dei contrari, forte e fragile, decisa ma malleabile. Grazie per avere fatto di me quella che sono oggi, grazie per ogni grande e piccolo momento passato insieme. Ti voglio un bene immenso, sei stata e sei il mio più grande punto di riferimento.

Grazie al mio papino, mio specchio riflesso. A volte mi stupisco di quanto ci assomigliamo, ma allo stesso tempo mi fa paura. Grazie per tutte le volte in cui mi hai spinto a dare il massimo, a non mollare mai, a spendere al meglio tutte le mie potenzialità e soprattutto a puntare in alto.

Grazie a Francesco, mio piccolo ma tanto grande falò che ha acceso tutta la mia vita con un fuoco brillante e perfetto nella sua imperfezione. Grazie per essere la parte migliore di me, grazie per essermi stato vicino in ogni momento e avermi sostenuta. Grazie per essere il mio migliore amico, il volto che cerco tra mille, la mia scelta quotidiana, semplicemente fondamentale.

Grazie a madri, mia seconda mamma. Grazie perché sei la mia roccia e il mio esempio. Grazie perché ogni giorno so di poter contare su di te sempre. Grazie per ogni momento, ogni chiacchierata, ogni discussione e incomprensione. Grazie perché mano nella mano con te sento che posso superare ogni ostacolo.

Grazie a Guido, che nonostante io conosca da poco ha colorato la nostra famiglia con sfumature nuove. Grazie perché con te tutto sembra semplice. Grazie perché con te sento di essere in famiglia.

Grazie a Pitti, l'amico di cui non credevo di avere bisogno. Grazie perché in questi anni hai saputo starmi vicino senza urlare, ma facendo un silenzio rumoroso. Sei per me il promemoria costante della tranquillità che racchiude forza che vorrei avere, ma su cui devo ancora lavorare.

Grazie a Fabietta, mia rosa. Grazie per avermi presa per mano quando non credevo più nell'amicizia e portata nel nostro magico mondo. Grazie perché i chilometri che ci separano non sono che lancette che scorrono per contare il tempo che separa il nostro incontro.

Grazie a Eva, mio braccio destro e qualche volta anche sinistro. Grazie per essermi stata accanto in questo tortoso percorso universitario. Grazie per i nostri caffè al MixTo, per tutte le ore passate assieme a studiare, a fare niente, a ridere o semplicemente a stare insieme. Sei stata e sei essenziale.

Grazie a nonna Muccia e nonno Fino, perle preziose che porto ogni giorno con me. Grazie perché seppur non abbiamo avuto la fortuna di passare abbastanza tempo insieme, siete stati capaci di lasciare un'impronta nella mia crescita che tutt'ora mi rende me stessa. Grazie perché guardando il cielo so che da lassù siete fieri di me e mi guardate con quello sguardo amorevole che solo voi sapevate far risplendere.

Grazie a nonno Mario e nonna Rinu, nonni pazzereelli ma pieni di dolcezza. Grazie perché il vostro amore costante mi fa crescere e mi rende più consapevole.

Grazie di tutto, vi voglio un bene immenso.

Grazie a Elisa e Marta, sorelle acquisite. Grazie per avermi sempre capita e aiutata. Grazie per il vostro esempio silenzioso ma presente. Grazie per tutte le merende e per i discorsoni sul futuro. Grazie per tutti i momenti passati insieme che porto nel cuore. Grazie per essere le sorelle che non avrei mai desiderato di avere.

Grazie alla mia famiglia, colonna portante della mia crescita. Grazie perché senza il vostro aiuto non sarei mai riuscita a superare i miei limiti e ad ottenere questi risultati.

Grazie ai Nipoti di Santina, amici ormai da quasi una vita. Grazie a Rebi, amica speciale che c'è stata e c'è per ogni mia pazzia. Grazie a Marta, la nostra diva, grazie perché rendi speciale ogni momento passato insieme. Grazie a Marti per avere sempre il consiglio giusto per tutti, soprattutto per me. Grazie a Kay che ogni tanto si butta giù ma solo perché non sa quanto vale e quanto significhi per me. Grazie a Cami che con la sua vena artistica colora il nostro gruppo con sfumature magnifiche. Grazie a Franci che con il suo esempio e la sua tranquillità sa mettere tutti a proprio agio. Grazie a Lollo per la sua pazza leggerezza, grazie per farmi sentire vecchia, ma soprattutto per farmi ridere anche quando non vorrei.

Grazie a Simo, maestra di danza e di vita. Grazie perché ci sei stata senza fare domande, grazie perché durante questi anni mi hai preso per mano e mi hai cresciuta come una figlia. Grazie per ogni sorriso e momento passato insieme. Grazie soprattutto per avermi capita e fatta crescere.

Grazie a Taina, che ha paura della luce, ma non si accorge di essere lei stessa luce. Grazie per avermi insegnato che i tagli che abbiamo sulla pelle ci rendono speciali e unici. Grazie per la tua forza, il tuo esempio, la tua consapevolezza. Grazie per avermi capita e incoraggiata.

Grazie ai miei compagni di Erasmus, toppe colorate sul mio zaino. Grazie perché durante questo anno in Belgio ho avuto la fortuna di condividere con voi questa esperienza bellissima. Un grazie particolare va a Martina ed Eleonora, grazie per tutti i calici di vino, per le birre, per i discorsi malinconici, per le serate, per le pedalate (queste sicuro non per Martina). Grazie perché avete reso questo anno indimenticabile.

Grazie a tutti coloro che ho incontrato durante l'università, professori, amici, volti indistinti tra i corridoi. Grazie perché anche se non ve ne siete resi conto, avete reso un po' più leggero questo arduo percorso.

Grazie a tutti i miei animati, piccole stelline più brillanti che mai. Grazie perché da voi ho ricevuto mille volte di più rispetto a quello che ho cercato di donare. Grazie per tutte le frasi inaspettate, le risate, i pianti, i silenzi, le discussioni. Grazie perché sono cresciuta con voi, fianco a fianco e siete uno dei miei più grandi orgogli.

Grazie ad Acceglio, mio posto del cuore. Grazie perché la magia di quel posto

speciale in cui ho pianto, riso, ragionato e in cui sono cresciuta ha forgiato la mia anima.

Grazie a tutti amici, parenti, conoscenti. Ogni volto, ogni parola, ogni momento è impresso a fuoco nel mio cuore e nella mia mente. Siete speciali. Sono così fortunata che un grazie non può certo bastare.

Table of Contents

List of Tables	XI
List of Figures	XIII
Acronyms	XVII
1 Introduction	1
1.1 Introduction on the anatomy of the gastrointestinal tract	1
1.2 Gastrointestinal tract investigation systems - State of the art . . .	2
1.3 Wireless capsule endoscopy - State of the art	4
1.4 Localization methods	6
1.4.1 Time of arrival and direction of arrival	9
1.4.2 Phase difference of arrival	9
1.4.3 Received signal strength	10
1.5 Effect of different human tissues on the localization methods	10
1.6 Thesis objective	11
2 Materials and methods	13
2.1 Antennas	13
2.1.1 Transmitting antenna	15
2.1.2 Receiving antennas	16
2.2 Body model	16
2.2.1 Duke properties	17
2.3 RSS calculation	19
2.4 Sim4Life simulation	20
2.4.1 Initialisation functions	20
2.4.2 Simulation	22
2.4.3 From Sim4Life data to numpy data	23
2.4.4 Extract electric field	23
2.5 Analysis	24

3	Results and discussion	27
3.1	Air model	29
3.1.1	Comparison between different locations inside the GI tract for the air model	29
3.1.2	Comparison between different Rx positions for the air model	33
3.2	Fat model	35
3.2.1	Comparison between different locations inside the GI tract for the fat model	36
3.2.2	Comparison between different Rx positions for the fat model	40
3.3	Muscle model	42
3.3.1	Comparison between different locations inside the GI tract for the muscle model	42
3.3.2	Comparison between different Rx positions for the muscle model	45
3.4	Duke model	47
3.4.1	Comparison between different locations inside the GI tract for the Duke model	48
3.4.2	Comparison between different Rx positions for the Duke model	52
3.5	Models comparison	53
3.5.1	Interpolation values	54
3.5.2	Input powers	56
3.5.3	Tx antenna electric field propagation	58
3.6	Localization error analysis	61
4	Limitations and future work	66
5	Conclusion	67
A	Simulation code	70
A.1	Definitions of the functions present inside the code	70
A.2	Main code	74
B	Data conversion code	78
B.1	From smash data to npy data	78
B.2	Extract electric fields	79
	Bibliography	84

List of Tables

2.1	Characteristic of the sphere around the antenna	14
2.2	Characteristic of the Duke model [29]	18
2.3	Properties of the Duke model at 868 MHz [29]	18
3.1	Electric field parameters for the air model in the positions illustrated in Figure 3.1	32
3.2	Values of maximum, minimum, mean, 25 th percentile, and 75 th percentile of the electric field in dB for different Rx positions for the air model	35
3.3	Electric field parameters for the fat model in the positions illustrated in Figure 3.1	38
3.4	Values of maximum, minimum, mean, 25 th percentile, and 75 th percentile of the electric field in dB for different Rx positions for the fat model	41
3.5	Electric field parameters for the muscle model in the positions illustrated in Figure 3.1	45
3.6	Values of maximum, minimum, mean, 25 th percentile, and 75 th percentile of the electric field in dB for different Rx positions for the muscle model	48
3.7	Electric field parameters for the Duke model in the positions illustrated in Figure 3.1	51
3.8	Values of maximum, minimum, mean, 25 th percentile and 75 th percentile of the electric field in dB for different Rx positions for the Duke model	54
3.9	Values of R ² for hyperbolic interpolation	56
3.10	Real part of the input power of the Tx antenna for the different body models	57
3.11	Values of maximum, minimum, range, 25 th percentile, 75 th percentile, and range P75-P25 of the distances [m] given an electric field [mV/m] calculated with the interpolation curve for the air model	62

3.12	Values of maximum, minimum, range, 25 th percentile, 75 th percentile and range P75-P25 of the distances [m] given an electric field [mV/m] calculated with the interpolation curve for the fat model	63
3.13	Values of maximum, minimum, range, 25 th percentile, 75 th percentile, and range P75-P25 of the distances [m] given an electric field [mV/m] calculated with the interpolation curve for the muscle model	63
3.14	Values of maximum, minimum, range, 25 th percentile, 75 th percentile, and range P75-P25 of the distances [m] given an electric field [mV/m] calculated with the interpolation curve for the Duke model	64
3.15	Range of error in distance and range between P75 and P25 for each body model	64

List of Figures

1.1	Gastrointestinal tract [2]	2
1.2	Variants of rigid endoscopes [5]	3
1.3	Flexible endoscope [4]	4
1.4	Assembly drawing of MC4000 a type of WCE on the market [10] . .	5
1.5	Scheme WCE localization methods	8
2.1	Antenna model	14
2.2	Radiation pattern of a dipole antenna	15
2.3	Modelling of the position of the Rx antennas	16
2.4	Duke model from Sim4Life	17
2.5	3D image of the path along with there are the positions of the antenna on the GI tract	21
2.6	2D image of the path along with there are the positions of the antenna on the GI tract	22
2.7	Scheme of placement of the electric field extraction points	24
2.8	3D positions where the electric field has been converted	25
3.1	Duke model with the four positions on the GI chosen for the analysis	28
3.2	Graph of distances between Tx and Rx and electric field for a location at the end of the esophagus for the air model	29
3.3	Graph of distances between Tx and Rx and electric field for a location in the small bowel for the air model	30
3.4	Graph of distances between Tx and Rx and electric field for a location at the beginning of the intestine for the air model	31
3.5	Graph of distances between Tx and Rx and electric field for a location at the end of the intestine for the air model	31
3.6	Magnitude of the electric field around the body for the air model in the four chosen locations (the end of the esophagus, in the small bowel, at the beginning of the intestine and at the end of the intestine) in dB scale	33

3.7	Graph of distances between Tx and Rx and electric field for the position 4 mm, 10 mm, 20 mm and -6 mm of the Rx antenna for the air model with their interpolation curve	34
3.8	Graph of distances between Tx and Rx and electric field for a location at the end of the esophagus for the fat model	36
3.9	Graph of distances between Tx and Rx and electric field for a location in the small bowel for the fat model	37
3.10	Graph of distances between Tx and Rx and electric field for a location at the beginning of the intestine for the fat model	37
3.11	Graph of distances between Tx and Rx and electric field for a location at the end of the intestine for the fat model	38
3.12	Magnitude of the electric field around the body for the fat model in the four chosen locations (the end of the esophagus, in the small bowel, at the beginning of the intestine, and at the end of the intestine) in dB scale	39
3.13	Graph of distances between Tx and Rx and electric field for the position 4 mm, 10 mm, 20 mm, and -6 mm of the Rx antenna for the fat model with their interpolation curve	40
3.14	Graph of distances between Tx and Rx and electric field for a location at the end of the esophagus for the muscle model	43
3.15	Graph of distances between Tx and Rx and electric field for a location in the small bowel for the muscle model	43
3.16	Graph of distances between Tx and Rx and electric field for a location at the beginning of the intestine for the muscle model	44
3.17	Graph of distances between Tx and Rx and electric field for a location at the end of the intestine for the muscle model	44
3.18	Magnitude of the electric field around the body for the muscle model in the four chosen locations (the end of the esophagus, in the small bowel, at the beginning of the intestine and at the end of the intestine) in dB scale	46
3.19	Graph of distances between Tx and Rx and electric field for the position 4 mm, 10 mm, 20 mm, and -6 mm of the Rx antenna for the muscle model with their interpolation curve	47
3.20	Graph of distances between Tx and Rx and electric field for a location at the end of the esophagus for the Duke model	49
3.21	Graph of distances between Tx and Rx and electric field for a location in the small bowel for the Duke model	49
3.22	Graph of distances between Tx and Rx and electric field for a location at the beginning of the intestine for the Duke model	50
3.23	Graph of distances between Tx and Rx and electric field for a location at the end of the intestine for the Duke model	51

3.24	Magnitude of the electric field around the body for the Duke model in the four chosen locations (the end of the esophagus, in the small bowel, at the beginning of the intestine, and at the end of the intestine) in dB scale	52
3.25	Graph of distances between Tx and Rx and electric field for the position 4 mm, 10 mm, 20 mm, and -6 mm of the Rx antenna for the Duke model with their interpolation curve	53
3.26	Comparison between the four models	55
3.27	Comparison between the four models normalized by the input power in dB scale	57
3.28	XY plane representation of the electric field through the Tx antenna orientated toward x, y, and z for the air model	58
3.29	XY plane representation of the electric field through the Tx antenna orientated toward x, y and z for the fat model	59
3.30	XY plane representation of the electric field through the Tx antenna orientated toward x, y, and z for the muscle model	60
3.31	XY plane representation of the electric field through the Tx antenna orientated toward x, y, and z for the Duke model	61
3.32	Graph of distances and electric field for the four models for localization purposes and their hyperbole interpolation	62

Acronyms

BMI

Body mass index

EM

Electromagnetic

FDA

US Food and Drug Administration

FDTD

Finite difference time domain

GI

Gastrointestinal

PEC

Perfectly Electric Conducting

PDoA

Phase difference of arrival

RF

Radio frequency

Rx

Receiver

RSS

Received signal strength

TDoA

Direction of arrival

ToA

Time of arrival

Tx

Transmitter

ViP

Virtual Population

WCE

Wireless capsule endoscopy

Chapter 1

Introduction

1.1 Introduction on the anatomy of the gastrointestinal tract

The gastrointestinal system (GI) is a very complex apparatus that, unlike others, occupies a large part of the human body. It consists of a muscular tube, called the digestive canal, and various accessory organs. The digestive canal is composed of the oral cavity (mouth), pharynx, esophagus, stomach, small intestine, and large intestine. Other accessory organs include the tongue, teeth, and various glands, such as the salivary glands the liver, gallbladder, and pancreas, which secrete water, enzymes, buffers, and other components into ducts that empty into the digestive canal (Figure 1.1). Food passes through the entire digestive canal and, during this journey, secretions prepare nutrients for absorption through the epithelium of the digestive canal [1].

The digestion starts in the oral cavity, where the chewing and insalivation of what forms the so-called bolus take place. This movement continues along the pharynx and esophagus with the swallowing process. The bolus moves to the stomach where both chemical and mechanical digestion takes place to form the commonly named chyme. In the small intestine, chemical digestion and absorption take place with the formation of the chyle. Finally, in the large intestine, there is the absorption and the stool formation.

Due to the fact that the GI is a very complicated and heterogeneous system, it may be affected by a large variety of diseases ranked from mild to severe. Accurately diagnosing digestive disorders involves collecting a thorough medical history and conducting examinations in order to treat the patients.

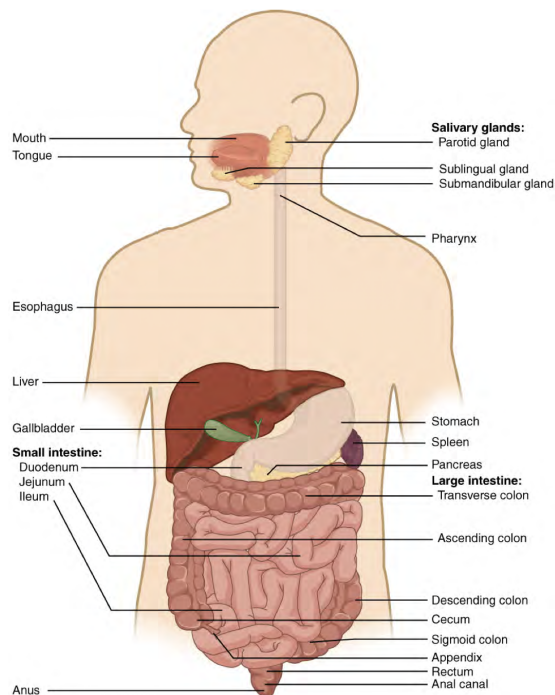


Figure 1.1: Gastrointestinal tract [2]

1.2 Gastrointestinal tract investigation systems - State of the art

Nowadays, gastrointestinal diseases such as bleeding, infections, cancer, inflammatory bowel diseases, and others remain a huge problem and a big threat to human health. In particular, gastric and colorectal cancer are ranked third and fourth in the mortality rate classification.

The traditional endoscope represents the gold standard for the examination of the gastrointestinal tract [3] which otherwise would be an inaccessible site. Endoscopes are instruments that use tubes that are only a few millimeters thick to transfer illumination inside the GI tract and high-resolution images in real time out of the body, resulting in minimally invasive surgeries or explorations. There are two types of endoscopes present on the market which are used in clinical practice:

- *Rigid tube endoscope* (Figure 1.2). There are different model variants but they are normally composed of an outer scope tube, the rigid body of the scope, a light guide that enable the surgeon to view inside the tract, an image interface, and a nosel. Normally it enters the human body through a surgical incision;
- *Flexible tube endoscope* (Figure 1.3). It is normally composed of a control

section that allows the surgeon to maneuver the instrument, the insertion tube that enters the body, and a tip that contains the lenses, the illumination system, and the image processor. Normally the examination, the diagnosis and, if necessary, the treatment, are performed through the natural orifices of the human body [4].



Figure 1.2: Variants of rigid endoscopes [5]

The problems the physicians may encounter when performing the examination of the GI with the endoscope are respectively:

- The *rigidity*. This is due to the fact that normally the endoscopes have four degrees of freedom which do not allow their full movement [6];
- The *bulky design*. Typically the endoscope is almost 160 mm in length and up to 14 mm in diameter;
- The possibility of *cross-contamination* of the liquids of different patients present on the device. In fact, it is common that if the sterilization is not performed correctly the instrument's channels are a perfect place for the proliferation and replication of pathogens. When the contaminated endoscope enters contact with a patient can cause several infections [7];
- The risk of *intestinal perforation*. The problem may occur mainly during interventional endoscopy while the probability is very low throughout a diagnostic

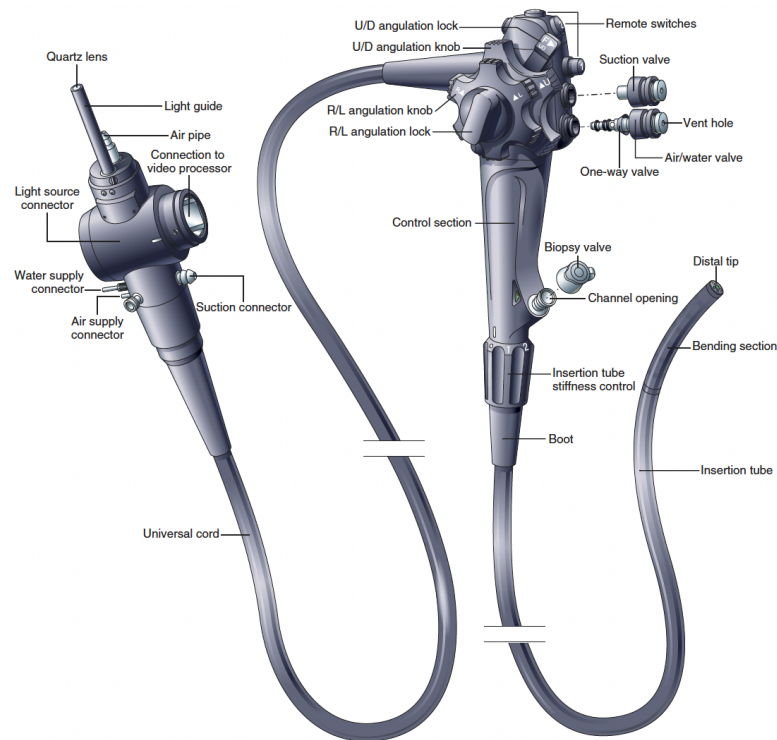


Figure 1.3: Flexible endoscope [4]

procedure [8];

- The *pain, discomfort* and *embarrassment* of the patient;
- The endoscope *does not allow examination of the whole GI*, because cannot investigate the entire small bowel.

In order to overcome all the problems listed above a new endoscopic method was first proposed in [9] in 1997 but approved by the US Food and Drug Administration (FDA) in 2001. The Wireless Capsule Endoscopy (WCE) was originally designed for small intestine imaging but nowadays is the only solution for the investigation of the whole GI tract.

1.3 Wireless capsule endoscopy - State of the art

Wireless capsule endoscopy is an innovative technology used for performing the examination of the GI system. Different from the traditional fiber-optical endoscopy, the patient is examined by swallowing a pill capsule which has the possibility to navigate through the GI tract in a non-invasive way and send images outside of

the body in order to be examined by the physician. In the original configuration, the WCE consists of a capsule-shape device equipped with:

- A *plastic shell*;
- One or more *cameras* for imaging acquisition;
- An *illuminating* system to make visualization of the internal organs possible;
- A *power source* to aliment the device;
- A *radio frequency* (RF) part containing an antenna and electronics useful for sending data outside the body.

The capsule (Figure 1.4) follows the gastrointestinal system from the esophagus to the colon, and the propulsion of the movement is achieved by peristalsis which is the natural contractions of the intestines. This movement is painless hence the patient is more inclined to accept it. During the mouth-to-evacuation period, the WCE measures signals and records images by multiple receivers, worn on (normally with a belt) or close to the body, and transmits them to a data recorder outside the body. The physician examines the recorded images searching for abnormalities.

This technique offers multiple benefits compared to conventional endoscopy, including non-invasiveness of the diagnosis, comfort for the patient, reach of all the organs in the GI tract, and time scale of the examination.

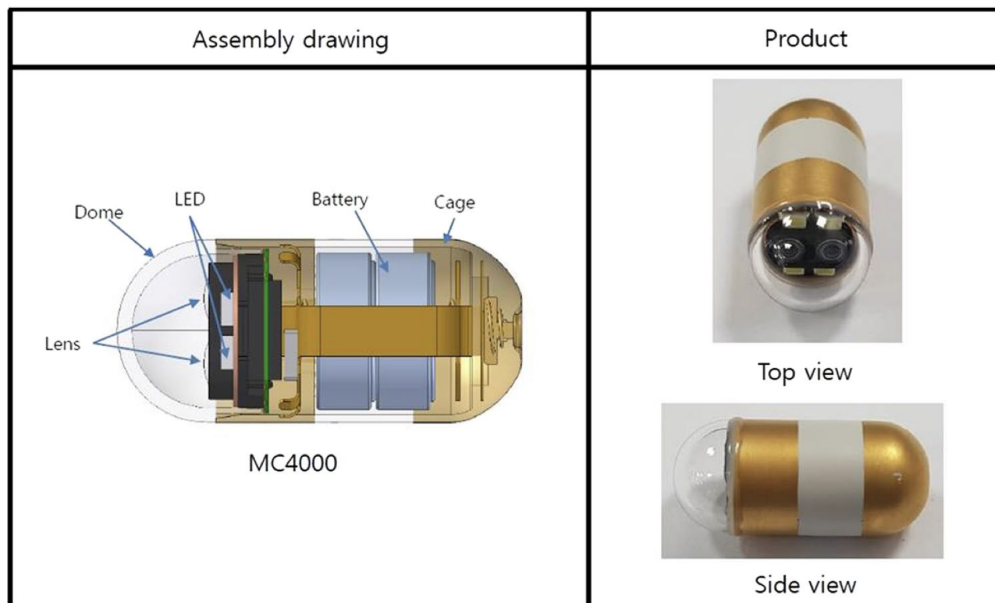


Figure 1.4: Assembly drawing of MC4000 a type of WCE on the market [10]

Notwithstanding the fact that the WCE has been proven successful in the detection of several diseases, there are some risks that need to be taken into account [11]:

- *Retention within the digestive tract:* This problem is the most dangerous. Studies have shown an occurrence of 3.1% enhanced in patients with motility disorders, suspected small bowel ulcers, or cancers. This is due to the fact that these diseases can easily influence the movements of the capsule [12];
- *Missed inspection:* The WCE uses a low frame rate for image capturing in order to reduce power consumption. However, this led to a small number of images in the possible lesion area, hence a potential missed inspection. Another cause of missed inspections can be due to a limited field of view of the capsule that cannot be moved by the physician as the traditional endoscope [13];
- *Blurred images:* The capsule is moving accordingly to the peristalses of the GI tract. In particular, WCE's motion is propelled when there is a muscle contraction, while it is decelerated during muscle relaxation. The difference in velocity can cause blurred images which can influence the diagnosis [14];
- *Localization problems:* The physicians cannot precisely locate the detected diseases because the localization techniques that are currently used in hospitals for tracking are definitively not precise [15].

Although WCE can provide images of the whole internal gastrointestinal tract, the identification of the exact location of the signals remains an open question. Location information is very crucial for the subsequent treatment of the detected diseases, either through local delivery of drugs or through surgery. The implementation of a reliable localization system is difficult also due to the complex electromagnetic (EM) environment within the human body. The huge potential of WCE in the future endoscopic field relies on the successful tracking of the wireless capsule.

1.4 Localization methods

Based on the research conducted until now, the tracking techniques used in medicine can be divided into three main sections:

- *Magnetic field-based* localization strategies. In magnetic field localization usually, the system that allows tracking the capsule is constituted by one or more magnetic sources called transmitter and one or more sensor modules called receivers. Either the transmitter or the receiver can be located inside

the capsule and, as a consequence, the other element will be situated outside the body [3]. The elements that are outside the body are normally either on the skin or in a belt worn around the waist. The sensors detect the magnetic field generated by a small magnet inside the capsule, and this information is used to determine the capsule's position and orientation. The main problems that characterize this technique are that the magnet occupies most of the space inside the capsule, and is very challenging to overcome the conflict between the actuation of the WCE and the localization system [16];

- *Visual-based* localization strategies. In visual-based localization, there are no additional sensors required. In fact, the position of the WCE is determined by calculating the velocity and evaluating the distance from certain anatomical landmarks, such as pylorus and ileocecal valve [17]. This technique uses computer vision algorithms to analyze the images captured by the capsule's camera and determine the position and orientation of the capsule within the GI tract. Visual-based localization techniques have several advantages over magnetic field-based techniques, such as not requiring external sensors and being able to provide a more detailed understanding of the capsule's surroundings. However, these techniques can be computationally expensive and may need significant processing power, which can be a challenge for real-time applications. Moreover, for the fact that the capsule is moving according to the peristaltic forces present in the GI, it is usually in motion and twisted. This makes it very difficult to track the capsule wireless using only the images [18];
- *Electromagnetic wave-based* localization strategies. EM tracking techniques make use of fields at different frequencies and known geometry to determine the position of the capsule inside the human body. In particular, a set of EM coils is placed outside the body, either on the skin or in a belt worn around the waist. These coils generate a magnetic field that interacts with a small coil inside the capsule. As the capsule moves through the GI tract, the magnetic field generated by the coils induces a voltage in the coil inside the capsule. The induced voltage is then measured by the coils outside the body and used to determine the position and orientation of the capsule [19]. Moreover, a more direct approach can be used. In particular, the antenna inside the capsule is used as a transmitting antenna and sends signals outside the body. In order to detect the signal produced, a series of multiple receptors are worn on the body [20]. However, some limitations have to be highlighted. In fact, this strategy suffers from limited precision and accuracy, especially in complex anatomical structures such as the small bowel or the intestine [21]. Actually, the signal is highly subjected to interference from the surroundings, leading to a complicated signal propagation, and as a result a higher error in

the localization [22]. Furthermore, it is often difficult to locate the endoscopic capsule due to the difficulty in reconstructing its position in the GI tract in three dimensions [23]. A further limitation is the continuous need for communication between the capsule and the external sensors in order to transmit the data obtained. In fact, this could induce uncontrolled battery consumption [3].

Electromagnetic wave-based localization strategies are the most adapted to localize medical targets. For this reason, this thesis will be limited to this technique.

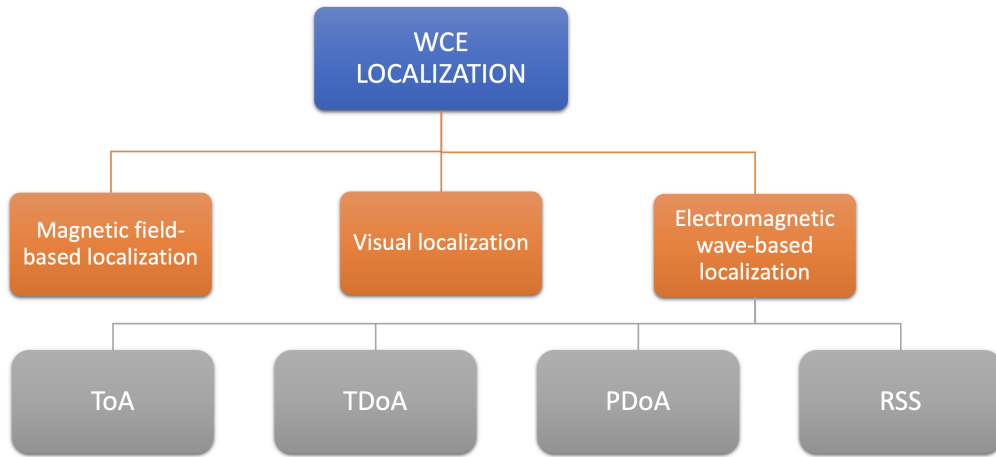


Figure 1.5: Scheme WCE localization methods

The current state of the art on endoscopic tracking systems with EM waves is mainly focused on using the radio frequency spectrum, which consists in wave between some Hz and 300 GHz. The basic theory of radio frequency localization is to use the propagation characteristic of the EM wave to calculate the distance and estimate the position based normally on triangulation. This is also due to the EM properties of the human body. In turn, the EM wave-based localization can be divided into:

- *Time of arrival* (ToA);
- *Direction of arrival* (TDoA);
- *Phase difference of arrival* (PDoA);
- *Received signal strength* (RSS);

1.4.1 Time of arrival and direction of arrival

Time of Arrival (TOA) is a technique that measures the time difference between when a signal is transmitted and when it is received at different receivers. By measuring the time delay of the signal, the distance between the transmitter and receiver can be calculated. Using multiple receivers, the location of the transmitter can be determined by triangulation.

Direction of Arrival (DOA) is a technique that estimates the angle or direction from which a signal is arriving at a receiver. This technique uses an array of antennas to measure the signal at each antenna and compare the phase and amplitude of the signal. By analyzing the differences between the signals received at each antenna, the direction of the signal can be estimated.

Although ToA and TDoA methods might be more accurate, according to literature, than the other RF methods (around 10 to 15 mm [24]), however, they require additional, costly, and unwieldy hardware, for example, for the synchronization system between transmitter and receiver and a particular array of antennas patterns. In addition, they also need an accurate knowledge of the propagation properties of the EM waves in passing through human tissue. Finally, there are some bandwidth limitations to consider [24].

1.4.2 Phase difference of arrival

PDoA can be used to estimate the location of the capsule within the GI tract by measuring the phase difference between signals received by multiple antennas placed on the body surface. As the capsule moves through the GI tract, the signals received at each antenna will have a different phase, due to the difference in the distance traveled by the signal to each antenna. By measuring the phase difference between signals received at different antennas, the direction of the capsule can be estimated. This type of localization strategy is probably the most difficult approach to analyze.

The accuracy of PDoA localization depends on several factors, such as the number and placement of antennas, the frequency of the signal, and the noise level in the environment. PDoA requires careful calibration and synchronization of the antennas to ensure accurate measurement of the phase difference.

Overall, PDoA is a promising technique for WCE localization that can provide accurate and real-time localization without the need for external sensors. However, it has been proven very inaccurate in heterogeneous models and for small wavelengths. Moreover, to be used in real applications it requires additional and costly hardware. In fact, the solution can be to use an iterative algorithm based on initial and coarse estimation [25].

1.4.3 Received signal strength

The Received signal strength (RSS) method consists of the measurement of the power present in the received radio signal. This localization technique is widely employed in localization processes in medicine. It is used to estimate the distance from a transmitter to a number of receivers. RSS-based localization can be achieved by measuring the strength of the RF signal transmitted by the capsule and received at each antenna. As the capsule moves through the GI tract, the strength of the signal received at each antenna will change due to the attenuation and absorption of the signal by the surrounding tissue. By measuring the RSS at multiple antennas, the location of the capsule can be estimated using different techniques. One approach that can be used consists of knowing the transmitted and received power and as a result, the path loss can be found. From a model, the distance can be estimated. Once the distances are obtained, the location can be found by multilateration. The principle could be to use the same radio frequency signal that the capsule uses to transmit images and video to transmit the localization signals. They can also use different types of radio frequencies to transmit the signals [26].

Radio Frequency modules are commonly used to localize the position of the capsule due to the intrinsic features of the RF signal. In particular, in terms of hardware, this technique is the easiest one, even though it has been established that possesses the largest localization errors. In literature, we can find errors from 30 to 100 mm ([11], [26] and [27]) depending on the stimulation frequency and the model that has been used for the study. Unfortunately, the RF signal attenuation through the human body is very high. Moreover, the results are strongly dependent on the carrier frequency, the number of receivers, the type of receiving antennas, and the complexity of the model, making the obtained results difficult to compare with other studies.

In order to improve the accuracy of the measurement the RF can be combined with other methodologies such as inertial unit measurement, visual imaging processing localization, machine learning, magnetic techniques, or exploiting the Kalman filter.

1.5 Effect of different human tissues on the localization methods

The human body consists of different tissue types. Each one of them has its own EM properties. In particular, permittivity and conductivity vary over different tissues and are dependent on the frequency of the EM wave of the transmitter and the receiver. These properties, affect the propagation of the EM wave inside and outside the body. Determining how EM waves travel inside the human body

over the different tissues is crucial for accurately determining the position and movement of the WCE along the GI tract.

In general, tissues with higher permittivity and conductivity, such as muscle and bone, will cause greater attenuation and scattering of the RF signal, resulting in a lower RSS at the receiving antennas. Conversely, tissues with lower permittivity and conductivity, such as fat, will cause less attenuation and scattering, resulting in a higher RSS at the receiving antennas [27].

The differences in permittivity and conductivity are determined, to a large extent, by the fluid content of the material. For example, blood and the brain conduct electric current relatively well. Lungs, skin, fat, and bone are relatively poor conductors. The liver, spleen, and muscle are intermediate in their conductivities. Differences in dielectric constants are more difficult to explain. The dielectric constant decreases and the conductivity increases with frequency.

In order to conduct an accurate study of the localization of the WCE along the GI tract, it is important to consider the different influences of each tissue. In particular, the interaction between the transmitting antenna and the receivers depends on the tissue that surrounds the capsule.

1.6 Thesis objective

The objective of this master's work is first to create a simulation program of the travel of the endoscopic capsule within the gastrointestinal tract. This is possible thanks to a finite difference time domain solver simulation on Sim4Life. Subsequently, a point conversion in terms of electric field and other parameters is required. In addition, most of the work involves comparing the influence of the localization of different tissues within the human body. Indeed, their different permittivity and conductivity characteristics lead to different results in terms of accuracy. After generating the results of the simulations varying these previous parameters, a thorough analysis has to be performed and comparisons between the different data have to be made. It is also important to understand which model creates the least uncertainty.

There have been implemented four simulations, three with models of the human body made up of only one homogeneous tissue and one with a completely heterogeneous model of the human body. Subsequently, it is crucial to understand how much each tissue affects the localization error. In order to achieve this goal, it is also necessary to understand how much the different parameters chosen are influenced by the tissue in question. For this reason, a series of comparisons are necessary. The main parameters that are taken into consideration throughout the GI tract are the values of the electric field and the distances between transmitter and receivers in plane and in space. Also fundamental, are the input power values

of the transmitting antenna according to which the electric field values have been normalized. This parameter is in fact indicative of how much the antenna influences the electric field values obtained. Furthermore, a location uncertainty analysis method was implemented. It is based on the maximum and minimum values of distances between the transmitter antenna and the receivers obtained given a small electric field interval.

Chapter 2

Materials and methods

In this thesis a numerical simulation technique was used to model the electromagnetic behavior of the wireless capsule endoscopy as it travels through the GI tract. In particular, the implementation was performed with finite difference time domain (FDTD) solver simulation on Sim4Life. Sim4Life is a simulation software package that allows the modeling of complex biological systems and the EM fields that interact with them. In order to implement the simulation, a program was written in Python language.

To conduct the simulation, a three-dimensional model of the whole body has been created using Sim4Life's modeling tools. This model includes anatomical features such as the size and shape of the body, as well as physiological properties such as the electrical conductivity and permittivity of the tissues.

The FDTD solver was then used to simulate the propagation of electromagnetic waves through the model, including the wireless signals transmitted and received by the capsule. The solver takes into account factors such as the capsule's position and orientation within the tract, as well as the properties of the surrounding tissues and fluids.

The simulation results can be analyzed to determine the location and orientation of the capsule at various points in time, as well as the strength and direction of the EM fields surrounding it. This information can be used to create a visual representation of the capsule's journey and the EM environment it encounters.

2.1 Antennas

In order to conduct the numerical simulation of the WCE along the GI tract, it is important to implement a source model in Sim4life. To this end, the dipole antenna was chosen. A dipole antenna is a type of radio antenna that consists of two conductive elements of equal length, that are aligned parallel to each other

and separated by a small gap. The two elements are often referred to as the "arms" or "legs" of the dipole. In particular, this type of source acts both as a transmitter (Tx) and as a receiver (Rx). Both transmitter and receiver are modeled as half-wavelength dipoles, consisting of two cylinders with a radius of 1 mm and a height of 3 mm. The two poles of the antenna are separated by 2 mm and fed by a line element as source [28]. The two arms of the antenna's material are the PEC (Perfectly Electric Conducting). This type of material has zero electrical resistivity and infinite relative permittivity. Due to these characteristics, it represents, as its name suggests, the perfect conductor which does not have any ability to store electrical energy and let electric current flow through it without any loss of energy. Moreover, a sphere that surrounds the entire antenna was implemented (Figure 2.1). It has a radius of 5 mm and has different relative permittivity if considered as a Rx or a Tx as can be seen in Table 2.1.

Characteristic	Value
Mass density	1000 kg/m ³
Electric conductivity	0 S/m
Relative permittivity Tx	97.2
Relative permittivity Rx	86.5

Table 2.1: Characteristic of the sphere around the antenna

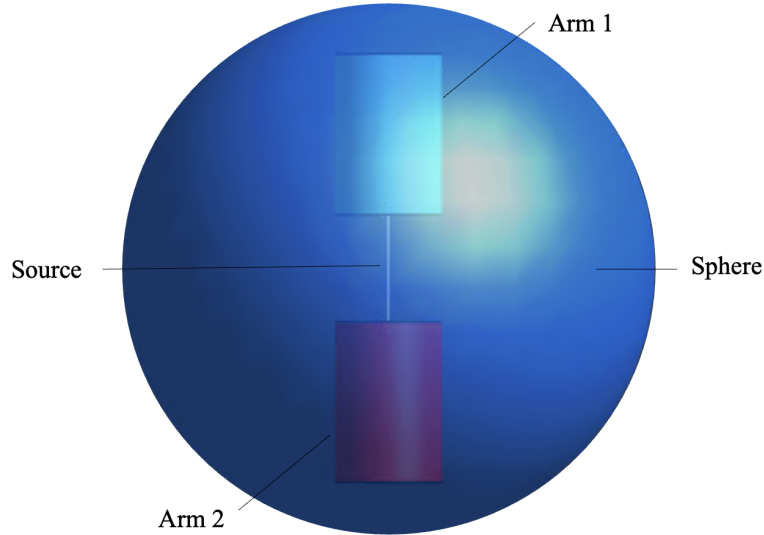


Figure 2.1: Antenna model

2.1.1 Transmitting antenna

The antenna model of the simulation radiate at 868 MHz which is in the bandwidth of the radio frequencies. From RF on, the electric and magnetic fields are coupled. This means that if an electric field exists, a magnetic field will be automatically produced. Therefore, one talks about electromagnetic fields.

The sources of these fields are both charges and currents. There is a relationship between current and charges which is based on the charge conservation law. This law states that the net change in the amount of electric charge in any volume of space is exactly equal to the net amount of charge flowing into the volume minus the amount of charge flowing out of the volume. It can be represented by the charge density continuity equation (2.1), where ρ is the charge density and J is the electric current density.

$$\frac{d\rho}{dt} + \nabla \cdot J = 0 \quad (2.1)$$

In order to correctly analyze the results it is important to understand the radiation pattern of the antenna. The source will not radiate in each direction equally. It will radiate more in some directions than in others as can be seen in Figure 2.2. This characteristic needs to be taken into account for the analysis of the results.

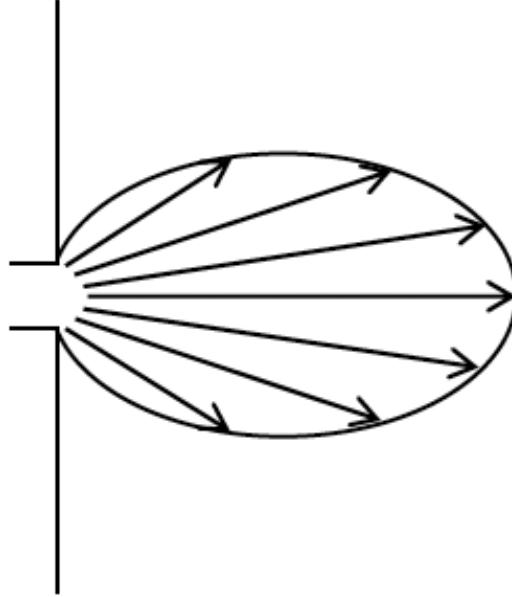


Figure 2.2: Radiation pattern of a dipole antenna

2.1.2 Receiving antennas

The receiving antennas are sensors that deal with the detection of the signal emitted by the Tx antennas. The number of Rx antennas and their placement with respect to the human body is essential in order to accurately track the capsule's movement through the GI tract. In this study, the Rx antennas were implemented as dipoles oriented parallel to the vertical axis of the body.

For what concerns the Rx antennas, in terms of numbers two different configurations were considered. In particular, twelve Rx antennas and sixteen. Analyzing the complexity of the simulation and the data obtained, they showed that the configuration with sixteen Rx is the most accurate. Nevertheless, it was decided to use the structure with twelve Rx in order to lighten the code and have a lower computational cost.

The positioning of the receivers, on the other hand, considered multiple configurations. However, the location of the receivers in the body area is always the same, in the abdominal area. What changes is the distance of the receivers from the body surface. In fact, distances varying from two to eighty millimeters were considered, both on the outside of the body and on the inside. In particular, the distances chosen are 2, 4, 6, 8, 10, 14, 20, 30, 50 and 80 mm from the skin of the model. As can be seen in Figure 2.3 there are therefore some receiver configurations inside the body represented in the image to the left (with a negative distance), and others outside as in the right image (with a positive distance).

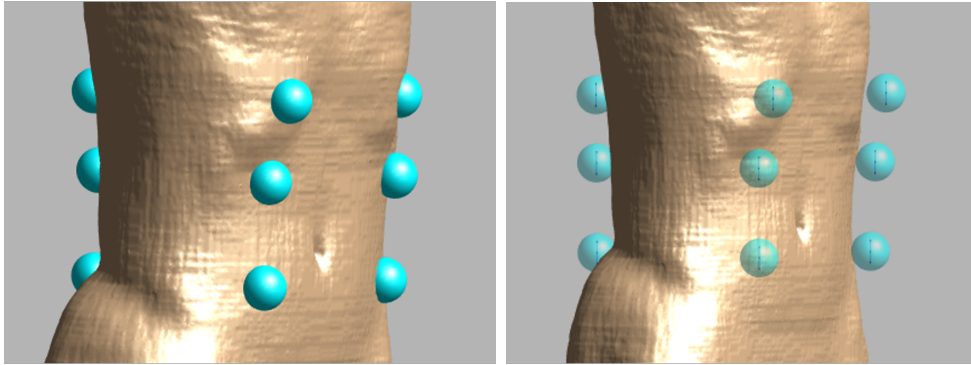


Figure 2.3: Modelling of the position of the Rx antennas

2.2 Body model

In order to replicate faithfully the anatomical GI an accurate human body model was needed. For this reason, Sim4Life provide a large set of Virtual Population

(ViP). The ViP is a set of body models, Duke is one of the heterogeneous models, representing an adult male. In this thesis the Duke model was chosen.

The ViP is a set of body models that replicate the human characteristics. This type of models are created using medical imaging data from real human subjects. There are different size and shape of these models including male and female adults, as well as children. The models are segmented into various tissue types, such as bone, muscle, fat, and others. This accuracy in modelling allows for detailed simulations of how electromagnetic fields interact with the human body [29].

In this thesis is was used the "Duke Adult Male" model (Figure 2.4), which is a high-resolution whole-body model of an adult male in his 30s. The characteristics of this body model can be seen in Table 2.2 where BMI stands for Body mass index.

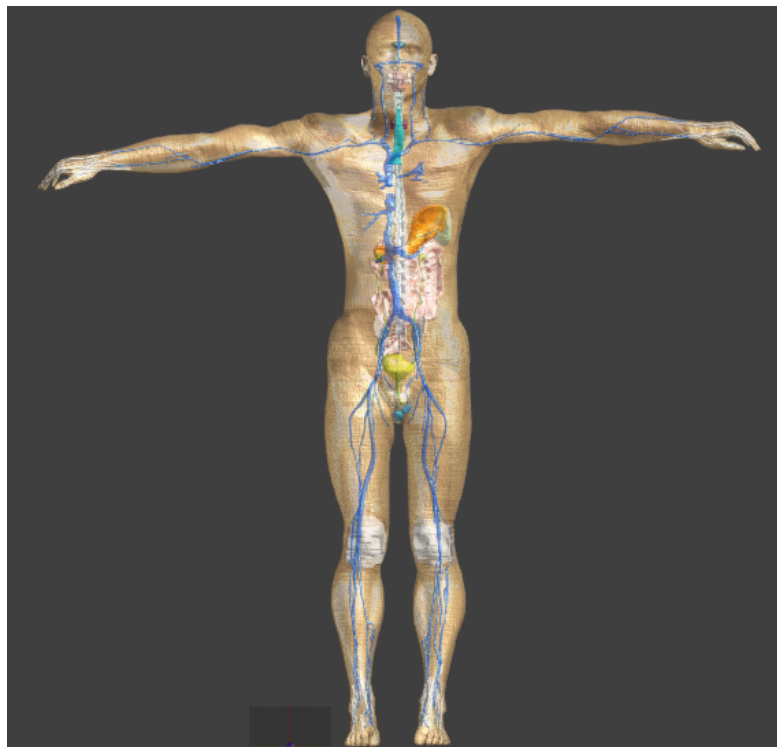


Figure 2.4: Duke model from Sim4Life

2.2.1 Duke properties

The conductivity and permittivity values of the ViP models vary depending on two important parameters:

- The specific tissue type or organ inside the human body;

Characteristic	Value
Name	Duke
Gender	Male
Height	1.77 m
Weight	72.4 kg
BMI	23.11 kg m^{-2}

Table 2.2: Characteristic of the Duke model [29]

- The frequency of the electromagnetic field which is chosen.

Some approximate values for a few of the tissue types at 868 MHz, frequency chosen for this work, (which is in the RF range) can be seen in Table 2.3.

For what concerned the air present inside the human body and around it, the permittivity value was approximated to the one of the vacuum ($8.854 \cdot 10^{-12}$ F/m). The conductivity, as the air is considered practically insulating, it can be approximated as 0 S/m.

Tissue	Conductivity [S/m]	Permittivity [F/m]
Muscle tissue	0.57	47.5
Adipose (fat) tissue	0.13	11.2
Bone tissue	0.019	12.8
Brain tissue	0.54	48.3

Table 2.3: Properties of the Duke model at 868 MHz [29]

Beneficial to understand better of the influence of the different tissues on the localization of the WCE and the relative accuracy, four different simulations have been performed. In particular, the various simulations have the objective of verifying which of the following configurations gives better accuracy in localization:

1. The "Duke Adult Male" model. It consists of all the modelization of the different organs with their specific EM properties. This is the most accurate and complex heterogeneous model analyzed. It takes a lot of time to consider all the different tissues and their properties during the simulation. Furthermore, due to the fact that Duke's model is very complex, made up of different tissues with different properties, it is often difficult to evaluate how much the various components influence the final result. For this reason, other configurations were implemented.
2. The homogeneous air model. This second model is the "Duke Adult Male"

where all the organs and the tissues have been set with the property of the air. This simulation can show us how the air inside our body interacts and influences the localization and the electric field inside and outside the human body.

3. The homogeneous fat model. This third model is the "Duke Adult Male" where all the organs and the tissues have been set with the property of the fat. This characteristic has the lowest permittivity among the tissues inside the human body. This simulation can give us an idea of how this tissue, which is strongly present inside the human body (in healthy subjects between 10-30% [30]) behaves. It is also essential to understand how the electric field propagates inside this type of tissue.
4. The homogeneous muscle model. This fourth model is the "Duke Adult Male" where all the organs and the tissues have been set with the property of the muscle. This tissue has the highest conductivity and almost the highest permittivity. The results can lead to a better interpretation of how all the parameters change in this type of tissue and how it affects the electric field inside the complexity of the entire human body.

2.3 RSS calculation

The RSS calculation is crucial to the estimation of the position of the capsule inside the body. It is the measurement of the strength of the signal received by sensors and transmitted by the capsule.

The method that has been implemented is called the maximum likelihood approach. It consists of finding the in-body Rx location that maximizes the probability of observing the measured RSS values based on an assumed empirical relation between RSS and distance. In particular, it works with the EM data fields generated by the different simulations. Moreover, the properties of the WCE simulated, such as orientation, location, and emission characteristics are used to estimate the localization.

For each of the Rx described before, the distance between the Tx and Rx antenna inside the WCE was calculated. This distance is crucial for estimating the RSS because the strength of an electromagnetic signal weakens as it travels through space. Afterwards, it has been taken into consideration the attenuation, scattering, and interference. These factors influence how the electromagnetic signal propagates from the WCE to the Rx. In fact, the RSS is reduced as it travels through biological tissues and encounters obstacles. Using the calculated distances and the signal propagation model, it has been estimated the RSS at each receiver location. This estimation represents how strong the electromagnetic signal is when

it reaches each receiver. Afterward, a localization algorithm is used to determine the probability of a location of the WCE. It has been considered the differences in RSS at various receivers to triangulate the WCE's position. It has been also calculated the probability distribution to quantify the probability of the position of the WCE.

2.4 Sim4Life simulation

With the goal of tracing the endoscopic capsule within the gastrointestinal tract, a Python program capable of simulating this pathway was created on Sim4Life.

2.4.1 Initialisation functions

With a view to best simulate the movement of the WCE in terms of translation and rotation, functions were initially implemented to reproduce these movements. In particular, there are three different functions that perform the rotation around each axis. In fact, there is a function that enables to perform the rotation around the x-axis, another one for the y-axis, and the last one for the z-axis. Moreover, there is a single function that allows the realization of the translations along all the axes.

In order to correctly transform the transmitting antenna to the desired location, a new function was implemented. It checks whether the Tx antenna is currently located at the origin and along the z-axis, which is called `basetransform` and it is a dictionary. This function is used to ensure that the Tx antenna is in the correct starting configuration before applying additional transformations to position it at a specific location and orientation for EM simulations. It helps maintain the consistency and accuracy of the simulation setup by starting with a known configuration for the antenna. In this way, there is also another function that could be used to verify whether an antenna's transformation has changed during the simulation or whether it matches a desired base transformation. This could be important for ensuring the accuracy of simulations and the proper positioning of antennas. It is also important to ensure that the antennas are positioned and oriented as required for specific simulations or scenarios. Also for this specific task, a function was created. It's a way to "reset" the transformations of the entities to specific configurations as opposed to applying incremental transformations.

After defining the processing functions of the antenna, it is important to specify the positions it takes along the GI tract. Three different functions were developed with this in mind. The first one generates a list of dictionaries of predefined antenna locations using fixed translation values for each antenna. It is important to define some step points. Each dictionary in the list is structured with a name which is the key to identifying the correct location and a transformation vector. There is a

second function that generates a set of antenna locations arranged in a grid pattern. Afterward, it calculates antenna positions based on the provided ranges for x, y, and z coordinates. The grid is formed by iterating through different combinations of x, y, and z values. Moreover, some conditions such as filtering and skipping specific combinations based on the name of the antenna are applied during this process. Each generated antenna location is stored as a dictionary in the list.

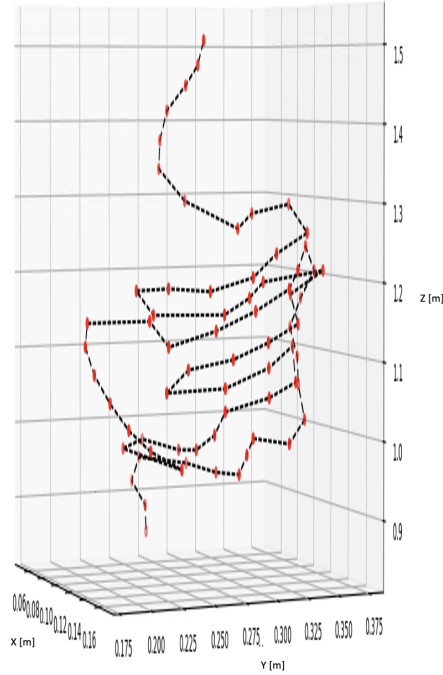


Figure 2.5: 3D image of the path along with there are the positions of the antenna on the GI tract

The last function generates antenna locations based on sixty-eight positions chosen in advance. Between each of these sixty-eight points, there is the calculation of ten additive points chosen by linear interpolation. For this reason, a total of six hundred and eighty points were used in order to specify the stops of the antenna inside the GI tract. The names of the points where the antenna is simulated are generated based on the iteration count and internal iteration count, providing a unique identifier for each location. In this way, it is also possible to find one single point separately. The path on which the points are chosen can be seen in Figure 2.5 and 2.6 in 3D and 2D respectively.

There is also a function that is responsible for the creation of antenna locations for the Fat model of the Duke. It consists of one hundred and four points since the Fat model of the Duke is bigger. In this thesis, this function was not used.

All the functions illustrated in this chapter can be found in Appendix A.1.

1. It checks at which point the simulation is working and saves the data of the current one. The code is made also to save a new copy of the file after some iteration in order to not allow the simulation file to become too large. In fact, after analyzing ten points, the simulation creates a new file.
2. Load the antenna model stored in another file and loop through each direction of rotation mentioned before. In fact, it reset the antenna position to the basetransform. Afterward, it applies the translation and the rotations.
3. Subsequently, there is the copy of the file and the orientation of the antenna. To them, a specific name is chosen. The label of the file is based on the level of the iteration and the position inside the GI tract.
4. The code updates the simulation's grid settings, adjusting padding based on the translation of the current location.
5. It then updates the simulation's grid settings and creates voxels.
6. The simulation is run using a specified server (wicasim4 in this case) or locally if no server is specified. After, there is the saving of the progress and the beginning of a new iteration.

All the code illustrated in this chapter can be found in Appendix A.2.

2.4.3 From Sim4Life data to numpy data

The resulting data obtained after the simulation finished running are in .smash format. They contained all the locations of the Tx antenna and their specific electric field. In this view, a new code was developed in order to transform the data we obtained from .smash into .npy file using the Analysis tab in Sim4life as can be seen in Appendix B.1. This type of format is definitively easier to handle and more compact in terms of space.

The electric field was extracted in a vector manner. In fact, the components along the x, y, and z-axis of the field were determined separately. In addition, the frequency of the electric field was derived.

2.4.4 Extract electric field

After making the simulation products lighter and more readable in .npy format, a new code had to be created to convert the data from .npy to .pickle. During this conversion, all parameters were precisely defined. The code can be found in Appendix B.2.

The first step was to extract the value of the electric field with some specific Rx distances with respect to the skin. In particular, the distances chosen are 2, 4, 6,

8, 10, 14, 20, 30, 50 and 80 mm from the skin of the model. These distances are calculated both positively and negatively. This means that the electric field was extracted for both external (positive) and internal (negative) Rx values.

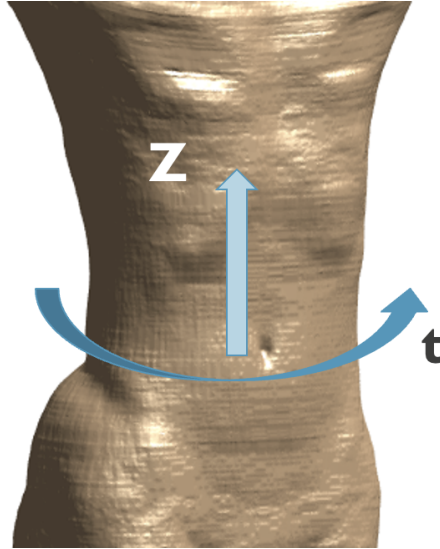


Figure 2.7: Scheme of placement of the electric field extraction points

The points where the electric field has been converted are positioned according to a precise geometry. In particular, they are located along circumferences moving on the vertical z -axis. In fact, there are forty-one points vertically where the conversion has taken place. Furthermore, along each of these forty-one vertical points, the electric field has been converted for sixty-three zones onward a circumference with a virtual radius. This contrivance makes it possible to convert points that lie exactly on the surface of the model's abdomen. These configurations can be seen in Figure 2.7 and 2.8.

The interpolated data are saved as pickle files in a directory structure based on distance and virtual radius. Each pickle file corresponds to a specific configuration and rotation vector. The electric field is saved in vector components along the Cartesian axes x , y , and z .

2.5 Analysis

From the various simulations carried out, many parameters have been obtained. In particular, the most relevant are those of the electric field within the GI tract and of the distance between Tx and Rx to which these values correspond.

From the parameters obtained, different variables were varied for each simulation, such as:

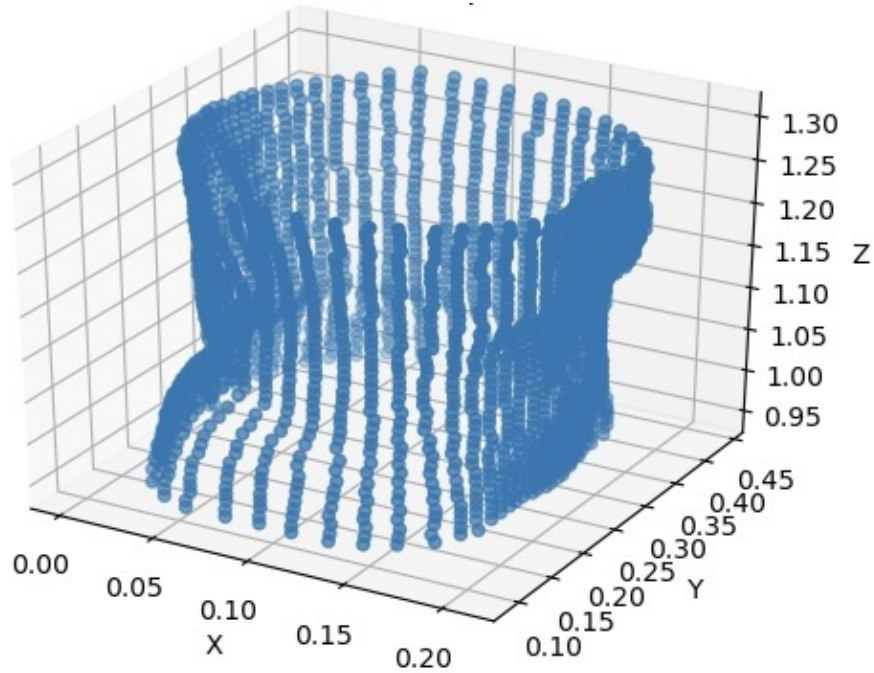


Figure 2.8: 3D positions where the electric field has been converted

- The type of body tissue used for the simulation;
- The location within the GI tract;
- The location of the Rx.

By varying these characteristics, the localization accuracy was analyzed. Following the conclusion of the simulations, the results obtained in terms of the electric field and the distance between Tx and Rx were extracted. This relationship is important as it is related to the location of the WCE. Theoretically, the relationship should be a decreasing hyperbolic function. In fact, where there are high field values, the distance between Tx and Rx will be smaller, vice versa when the field is bigger.

For each of the four simulated models (the three homogeneous models of air, fat and muscle respectively, and the heterogeneous complete Duke model), four positions within the GI tract were considered. Specifically, these locations are at the end of the esophagus, in the small bowel, at the beginning and end of the intestine. In these locations, the Rx position and the capsule orientation were kept constant, precisely 2 mm external to the body and parallel to the vertical axis of the body. In order to quantify the uncertainty, several parameters were calculated. These are respectively the maximum, minimum and mean value of both the electric

field and the distances between Tx and Rx obtained. In addition, the 25° and 75° percentile values of the obtained electric field were calculated.

Furthermore, it was important to find a suitable interpolation of the data. Several curves were considered, but the most suitable relationship was the hyperbolic one. A hyperbolic interpolation was therefore carried out for each simulation and for each point on the GI tract. In addition, the R^2 parameter was calculated in order to quantify the uncertainty. The R^2 provides a measure of the total variability in the data that is explained by the regression model. This parameter was also useful for comparing the results obtained for the different simulations.

Subsequently, the data obtained for different Rx positions for each of the four simulations were analyzed. In fact, all the analyses described above for the various locations along the GI tract were also performed at the position at the end of the esophagus, but for all Rx possible positions. In addition, both positive and therefore external locations were considered, as well as negative and so internal locations.

In addition, different input powers of the Tx antenna were analyzed for the comparison of the data obtained. These values were used to make it easier to compare the data obtained for the different tissues. The electric field values for each tissue were divided by the square root of the input power of the antenna. Then, the data were compared.

Moreover, for each of the simulations obtained, holding constant the point along the GI tract at the end of the esophagus and the position of Rx at 2 mm outside the body, the electric field in the presence of the Tx antenna with different rotations was evaluated. In fact, the antenna can assume a rotation parallel to the x-, y- or z-axis. In fact, the electric field around the Tx antenna varies according to the tissue surrounding it and according to its orientation.

Finally, a localization process has been implemented. Specifically, the results obtained for different points within the GI tract were merged for each simulation separately. The position of Rx was also kept constant and precisely 2 mm outside the body and the orientation of the capsule was parallel to the vertical axis of the body. Then, a hyperbolic fit curve was created by merging the electric field and distance values between Tx and Rx. This curve is therefore representative of the relationship between the electric field and the distance between Tx and Rx for each simulation. Subsequently, three constant values of distance between Tx and Rx were chosen. For each of these, through the interpolation curve, the interpolated electric field has been calculated. For this value, a range has been selected. In this interval of values, all distances between Tx and Rx that are in this range have been found. For each interval, the maximum, minimum, 25th and 75th percentiles and their difference were calculated. With these parameters, it was possible to calculate the uncertainty in the localization for each model analyzed.

Chapter 3

Results and discussion

After creating the code with which the simulation was launched, a detailed analysis of the result was carried out. In particular, the study was performed for each of the different models used (homogeneous of air, fat, and muscle and heterogeneous of the whole Duke). Additionally, a comparison between each different results was accomplished.

The first step in the analysis was to evaluate the different results obtained in different positions within the GI tract. This is because this parameter has a crucial impact on the localization for the presence of different tissues along the GI tract. Therefore, four positions were chosen (Figure 3.1), which are:

- At the end of the esophagus;
- In the small bowel;
- At the beginning of the intestine;
- At the end of the intestine.

The analysis was performed in terms of the range of values, hence considering the maximum and minimum values of distances and electric field obtained. Furthermore, the mean value, which is indicative of the average distance at which the capsule is placed is important for comparison between different data. The 25th and the 75th percentile have been also calculated. The parameters that were kept constant during this evaluation are the position of the Rx antennas and the orientation of the WCE. In particular, the first value was set at 2 mm external to the body model and the second one was along the z-axis which is the one parallel to the vertical axis of the body.

It was also essential to consider how faithfully the data obtained could be interpolated as an hyperbola. Indeed, if this curve was representative of the

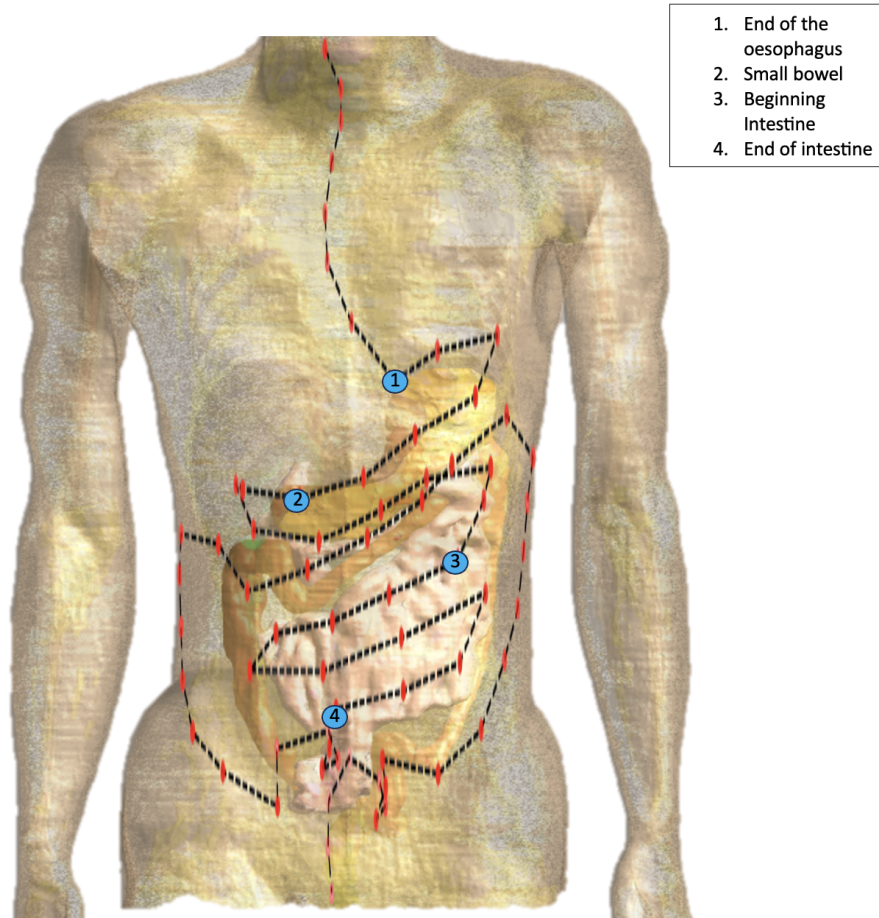


Figure 3.1: Duke model with the four positions on the GI chosen for the analysis

relationship between the distance between Tx and Rx and the electric field, it would be possible, given the electric field, to easily derive the distance.

It was crucial to investigate, for each simulation, the influence of the position of the Rx antennas on the chosen parameters. In this way, this important variable can be optimized. The data at all different Rx positions (2, 4, 6, 8, 10, 14, 20, 30, 50 and 80 mm internal and external to the body surface) have been extracted. In particular, the range of values, mean value and R^2 for the hyperbole interpolation for the distance between Tx and Rx and electric field were analysed at the location at the end of the esophagus.

Moreover, comparisons were made between the results obtained. In particular, the different electric field values in the homogeneous and heterogeneous models were compared. Furthermore, their interpolation with a hyperbolic curve was evaluated.

Subsequently, the values were compared taking into account the input power

of the Tx antenna. This process was done to eliminate the bias given by this parameter. Then a study on the propagation of the electric field around the Tx antenna was carried out. Finally, an error localization and evaluation process was conducted. Electric field values that were transformed from linear to decibel scale used a reference value of 1 V/m unless otherwise specified. Furthermore, the behaviors of the WCE were studied when the latter is oriented along the z-axis, which is the axis parallel to the vertical line of the body.

3.1 Air model

This section is dedicated to the stimulation of the journey of the WCE capsule inside the GI tract with the homogeneous air model. It consists of the Duke model, where all the materials of which the model was made are changed into air (Permittivity $8.854 \cdot 10^{-12}$ F/m and conductivity almost 0).

3.1.1 Comparison between different locations inside the GI tract for the air model

In the four locations mentioned before (at the end of the esophagus, in the small bowel, at the beginning of the intestine, and at the end of the intestine which can be seen in Figure 3.1) the relationship between Tx and Rx and the electric field was analyzed.

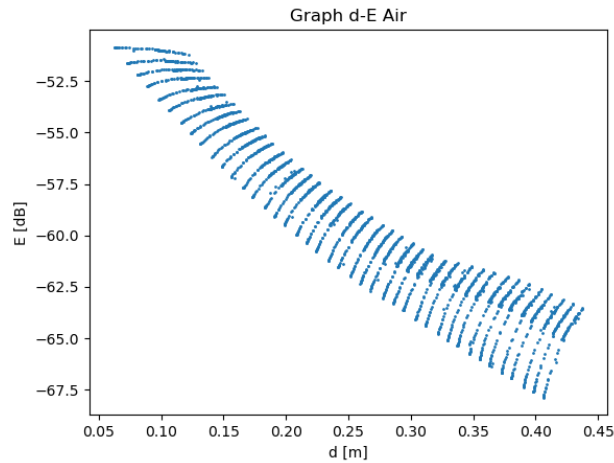


Figure 3.2: Graph of distances between Tx and Rx and electric field for a location at the end of the esophagus for the air model

Figure 3.2 shows the connection between the distance between Tx and Rx and

the electric field at the end of the esophagus. It can be seen that the minimum value represented in the distance between Tx and Rx is 0.0625 m and the maximum is 0.4375 m. The average value is 0.2518 m. It can be seen that as this distance between Tx and Rx increases, the electric field decreases almost uniformly. In fact, there is not much variability in the data.

If it were to interpolate the data with a hyperbola, the R^2 value would be 0.7725. This value of R^2 indicates that the results obtained are very close to the interpolation of the hyperbola.

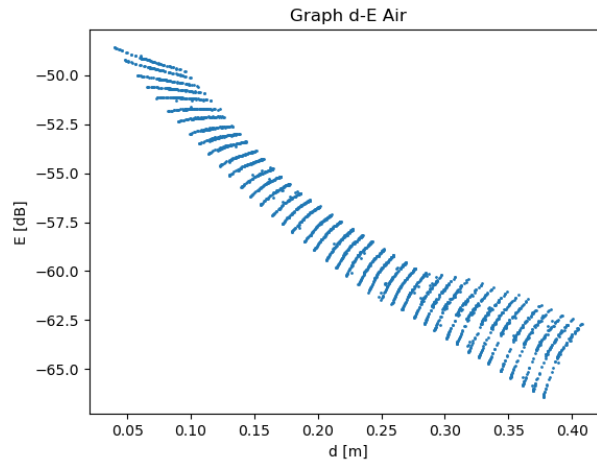


Figure 3.3: Graph of distances between Tx and Rx and electric field for a location in the small bowel for the air model

The dependency of the distance between Tx and Rx and the electric field in the small bowel has been depicted in Figure 3.3. It can be seen that the minimum value represented in distance between Tx and Rx is 0.0058 m and the maximum is 0.3581 m. The lowest value is lower than the previous one as well as the highest. For this reason, the range of values has shifted slightly downwards. The average value is 0.1760 m, which is smaller than the one preceding since the range of values is also smaller. It can be seen that, as the distance increases, the electric field decreases similar to the one at the end of the esophagus (Figure 3.2).

The interpolation of the data with a hyperbola generates an R^2 value of 0.7984. This value of R^2 indicates that the relation between the obtained data and the hyperbola is still high and higher than the previous one. In fact, there is lower variability around the mean value of the distance. Moreover, even around the maximum value, the discrepancy is reduced.

When considering a point at the beginning of the intestine, the result can be seen in Figure 3.4. The minimum value of distance between Tx and Rx is 0.0050 m and the maximum is 0.3580 m. This range of values is almost the same as the one

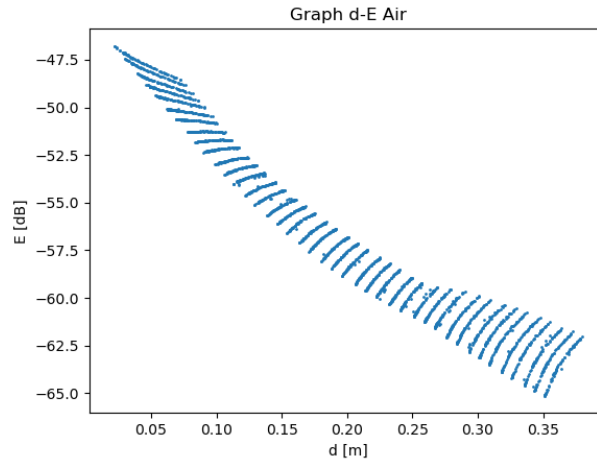


Figure 3.4: Graph of distances between Tx and Rx and electric field for a location at the beginning of the intestine for the air model

in the small bowel. The average value is 0.1760 m which is the same as the former one.

Interpolating the data with a hyperbola generates an R^2 equal to 0.7988. This value is very similar to the one for the small bowel. In fact, both the range, the mean value, and the shape of the plot are comparable.

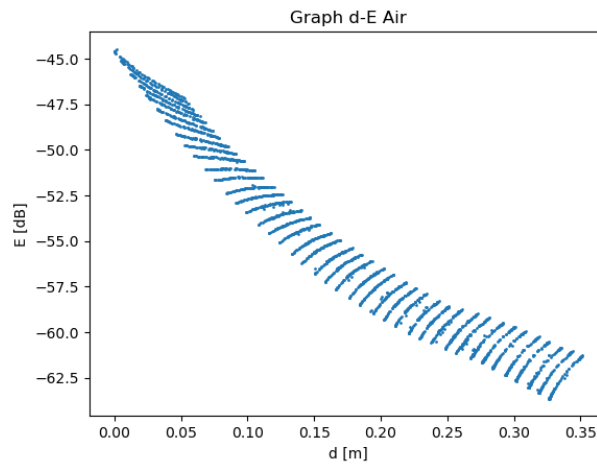


Figure 3.5: Graph of distances between Tx and Rx and electric field for a location at the end of the intestine for the air model

As for the location at the end of the intestine, it is depicted in Figure 3.5. The

minimum value of distance between Tx and Rx is 0.0057 m and the maximum is 0.3582 m. This range is comparable with the previous two. The mean value is 0.1760 m which is equal to the two preceding.

The interpolation of the curve with an hyperbola, generate an R^2 of 0.7998. This value is similar to the one for the small bowel and for the beginning of the intestine. It is slightly higher because the last part of the plot is more compact in values.

Position	Max E [dB]	Min E [dB]	Mean E [dB]	P25 [dB]	P75 [dB]
1	-49.06	-67.88	-59.12	-62.66	-55.52
2	-48.58	-66.40	-57.80	-61.68	-53.98
3	-46.80	-65.12	-56.66	-60.82	-52.66
4	-44.48	-63.64	-55.20	-59.64	-51.04

Table 3.1: Electric field parameters for the air model in the positions illustrated in Figure 3.1

The parameters calculated for the electric field can be seen in Table 3.1. It can be seen that there is no great variability between the data obtained in the four positions analyzed. The electric field in the different positions analyzed extends between very similar maximum and minimum values. Furthermore, the other calculated parameters are also similar to each other.

In Figure 3.6 it can be seen the magnitude of the electric field around the body in a plane representation. It can be appointed that the electric field, represented by the color code in the dB scale, is almost similar in the four areas analyzed. Particularly, the electric field, which is represented by the color code in the dB scale, is almost similar in the four areas investigated. In fact, there is an area at the top of the graph where the electric field is higher for the air model. In addition, as we move downwards, the electric field value decreases almost constantly.

One would have expected that there would be no variability at all between the results obtained along the GI tract of the homogeneous air model in terms of electric field and distances between Tx and Rx. In fact, since air has zero conductivity, it shouldn't present differences. However, due to the antenna model used and the different distances between Tx and Rx observed, there are minimal variations in the electric field in the four positions taken into consideration. Furthermore, there should be variations in the TZ plot due to the way the antenna radiates. In the resulting graph, there are variations, but not that important.

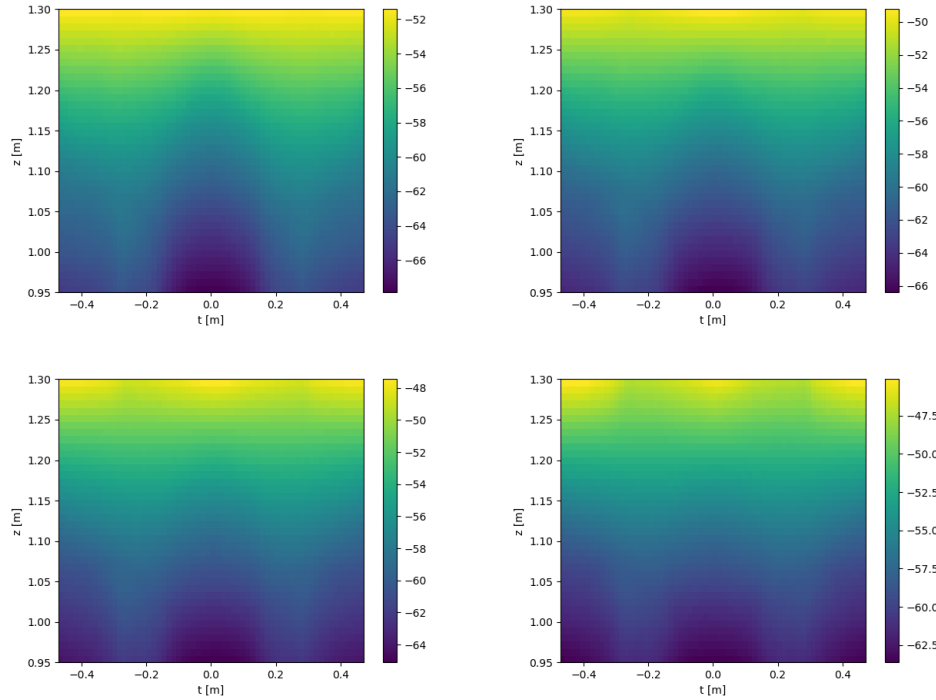


Figure 3.6: Magnitude of the electric field around the body for the air model in the four chosen locations (the end of the esophagus, in the small bowel, at the beginning of the intestine and at the end of the intestine) in dB scale

3.1.2 Comparison between different Rx positions for the air model

The study was conducted at the end of the esophagus, as mentioned before, for all the possible configurations of Rx (both internal and external to the body) with an orientation of the capsule along the z -axis. In particular, it can be seen in Figure 3.7 some of the relationships between the distance between Tx and Rx and the electric field for different positions of Rx. It is also shown in this image the interpolation curve which is a hyperbole and their specific equation. In addition, the electric field parameters can be seen in Table 3.2.

For what concerns the analysis of the distances of the Tx and Rx, it can be said that, apart from positions 30, 50, and 80 where the range is more shifted towards higher values, for the others the range between the minimum and maximum of the distances between Tx and Rx is almost constant. The average value also does not vary particularly much. In fact, the shape of the curve does not change substantially.

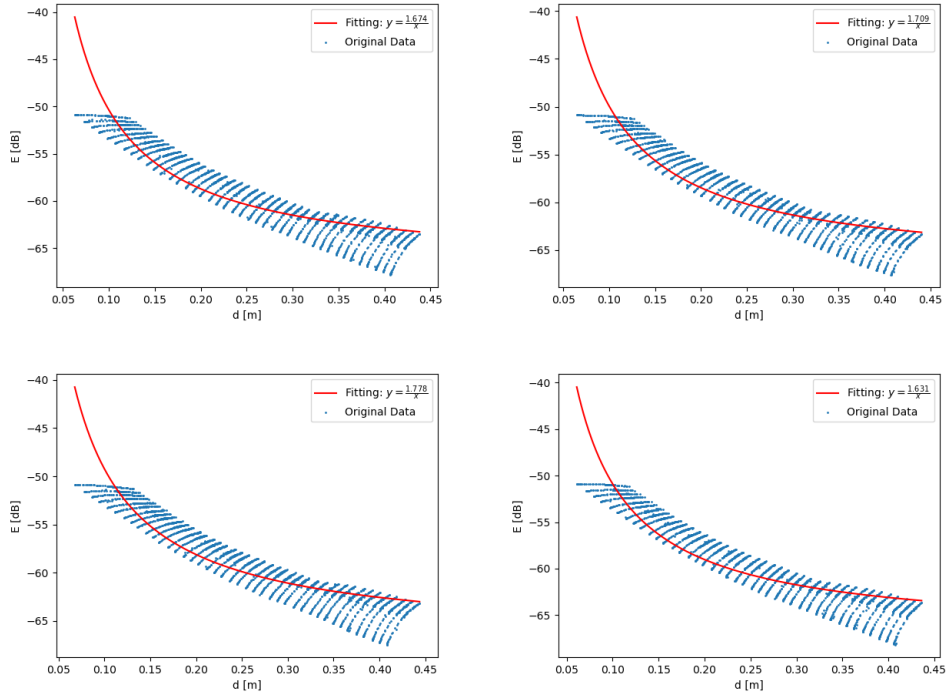


Figure 3.7: Graph of distances between Tx and Rx and electric field for the position 4 mm, 10 mm, 20 mm and -6 mm of the Rx antenna for the air model with their interpolation curve

th

If the parameters calculated on the electric field are analyzed (Table 3.2), it can be stated that for most of the distances between Tx and Rx, the field extends between values equal to -67 dB and -50 dB. The minimum value for distances equal to -50 mm and -80 mm is slightly higher. Furthermore, the calculated percentiles (25th and 75th percentiles) do not undergo particular variations.

From this analysis, it can be deduced that the position of Rx does not substantially influence the distance values between Tx and Rx and the electric field obtained for the homogeneous air model. In fact, the data does not undergo significant changes. Furthermore, in this case, there is not even a substantial difference between positions of Rx inside and outside the body. It can also be stated that for the air model, the hyperbola is an adequate interpolation since the results obtained follow the curve quite faithfully. In fact, in the relationship between the distance between Tx and Rx and the electric field, for this model, an almost hyperbolic decrease can be noted. For the homogeneous air model, the position

Rx dis [mm]	Min E [dB]	Max E [dB]	Mean E [dB]	P25 [dB]	P75 [dB]
2	-67.88	-49.06	-59.12	-62.66	-55.52
4	67.82	-50.86	-59.08	-62.06	-55.50
6	-67.68	-50.92	-59.04	-62.56	-55.46
8	-67.62	-50.88	-59.00	-62.50	-55.44
10	-67.58	-50.86	-58.96	-62.46	-55.42
14	-67.52	-50.88	-58.90	-62.38	-55.34
20	-67.44	-50.88	-58.80	-62.22	-45.48
30	-67.26	-50.90	-58.62	-61.98	-55.16
50	-66.60	-50.90	-58.32	-61.58	-54.98
80	-65.62	-50.94	-46.10	-61.04	-44.76
-2	-67.94	-50.86	-59.18	-62.72	-55.54
-4	-68.00	-50.86	-59.20	-62.78	-55.56
-6	-68.18	-50.86	-59.24	-62.82	-55.58
-8	-68.14	-50.86	-59.28	-62.88	-55.62
-10	-68.18	-50.86	-59.32	-62.94	-55.66
-14	-68.26	-51.02	-59.40	-63.04	-55.64
-20	-68.28	-51.38	-59.56	-63.18	-55.78
-30	-67.94	-51.96	-59.80	-63.46	-55.94
-50	-67.24	-53.24	-60.30	-64.06	-56.30
-80	-66.08	-55.38	-60.96	-64.82	-56.20

Table 3.2: Values of maximum, minimum, mean, 25th percentile, and 75th percentile of the electric field in dB for different Rx positions for the air model

of Rx relative to the body surface does not particularly influence the relationship between the electric field and the distance between Tx and Rx. Furthermore, an almost hyperbolic relationship of the decrease of the electric field with increasing distance between Tx and Rx was observed.

3.2 Fat model

This section is dedicated to the stimulation of the journey of the WCE capsule inside the GI tract with the homogeneous fat model. It consists of the Duke model, where all the materials of which the model was made are changed into adipose tissue (Permittivity 11.2 F/m and conductivity 0.13 S/m).

3.2.1 Comparison between different locations inside the GI tract for the fat model

The analysis of the correlation between the electric field and the distance between Tx and Rx for the fat model was conducted at the same locations as for the air model.

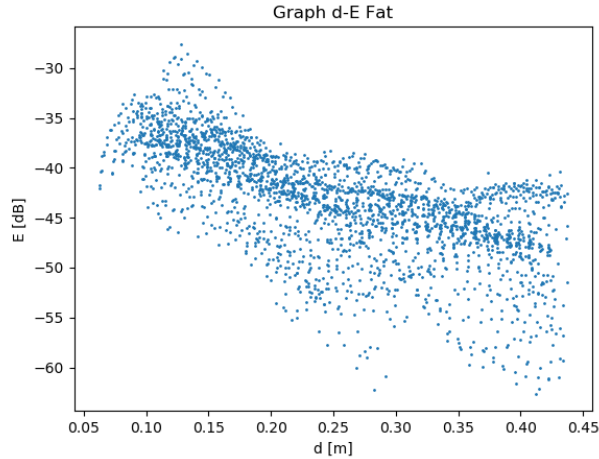


Figure 3.8: Graph of distances between Tx and Rx and electric field for a location at the end of the esophagus for the fat model

If we analyze this relationship at the beginning of the esophagus (Figure 3.8), it can immediately be seen that it is different in shape from the one in the homogeneous air model. Moreover, the range of electric field value is slightly higher. It can be claimed that the curve decreases in electric field values as the distance increases but with greater variability than in the previous analysis. In particular, the range of distances between Tx and Rx extends between a minimum value of 0.0625 m and a maximum value of 0.4375 m. The average value in this case is 0.2518 m. Thus, in contrast to the shape of the graph, the range in distances and the average value is very similar to the one conducted in air.

Furthermore, if one interpolates the curve with a hyperbola, the value of R^2 turns out to be 0.6247, which is slightly lower than in the previous model, but still comparable.

If one refers to the point in the small bowel, the plot can be found in Figure 3.9. The range of values in distances between Tx and Rx, in this case, extends between a minimum value of 0.0397 m and a maximum of 0.4083 m. The average value is 0.2216 m. These values are lower than at the end of the esophagus. However, the maximum and minimum values of the electric field do not undergo substantial variations compared to the previous point.

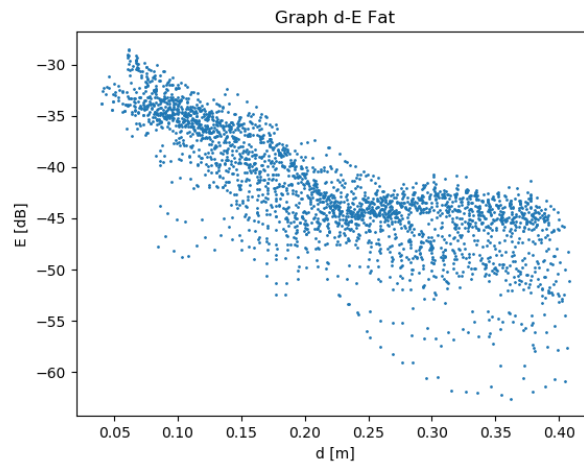


Figure 3.9: Graph of distances between Tx and Rx and electric field for a location in the small bowel for the fat model

The value of R^2 is 0.6890, which is slightly higher than the previous one, but of the same order of magnitude.

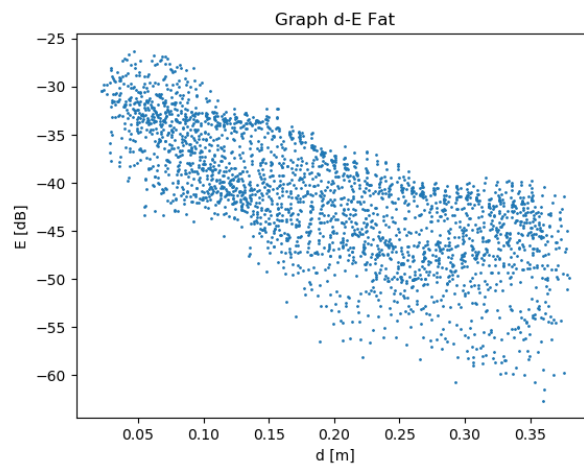


Figure 3.10: Graph of distances between Tx and Rx and electric field for a location at the beginning of the intestine for the fat model

For the location at the beginning of the intestine, the corresponding Figure is 3.10. The minimum value represented in the distance between Tx and Rx is 0.0219 m, while the maximum value is 0.3801 m. This range is still lower than the one in the small bowel. But, the average value is 0.2216 m which is the same as the

one previously obtained. The minimum electric field value obtained in this case is slightly lower than in the two locations analyzed previously, while the maximum is very similar.

As for the value of R^2 with a hyperbole interpolation, it amounts to 0.6090. It is slightly lower than the previous one. In fact, the points in the plot are less localized and more spread compared to the previous position.

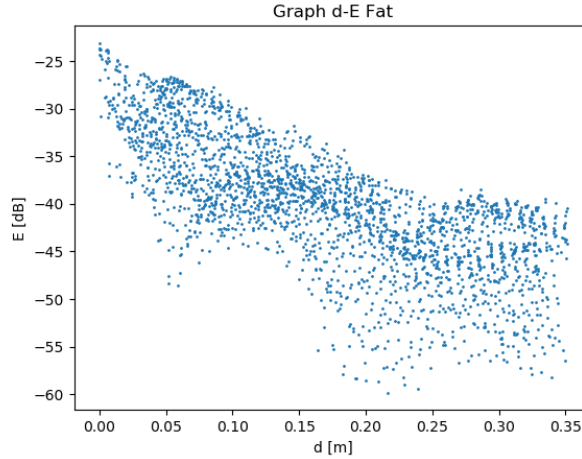


Figure 3.11: Graph of distances between Tx and Rx and electric field for a location at the end of the intestine for the fat model

The values obtained at the end of the intestine can be found in the Figure 3.11. The minimum value in distance between Tx and Rx is 0.0001 m, while the maximum is 0.3514 m. This range of distances is the minimum obtained so far. The average value is also low and equal to 0.1700 m.

The R^2 for this case amounts to 0.6102. If we compare it to the previous fat model it is in line with the others. This is due to the fact that the plot is similar in shape with the previous ones.

Position	Max E [dB]	Min E [dB]	Mean E [dB]	P25 [dB]	P75 [dB]
1	-27.62	-62.62	-43.36	-46.64	-39.36
2	-28.52	-62.60	-42.18	-45.48	-37.40
3	-26.34	-62.62	-41.68	-46.16	-36.92
4	-23.10	-59.82	-40.14	-44.52	-35.98

Table 3.3: Electric field parameters for the fat model in the positions illustrated in Figure 3.1

In Table 3.3 the electric field values obtained for the four considerate positions and the respective analyzed parameters can be found. It can be deduced that the electric field, also in this case, does not undergo particular variations, as well as the calculated values. The only electric field values slightly lower than the others are those obtained for the position at the end of the intestine. As regards the maximum value of the electric field, compared to that obtained for the homogeneous air model (Table 3.1), the one for the homogeneous fat model is much higher.

In Figure 3.12 it can be seen the magnitude of the electric field around the body in a plane representation for the homogeneous fat model. It can be stated that high electric field values are found in the upper part of the plot. Unlike the results obtained for the air model, there is no constant decrease in this case. In fact, moving horizontally one passes from medium-high values to other low ones within the observed range.

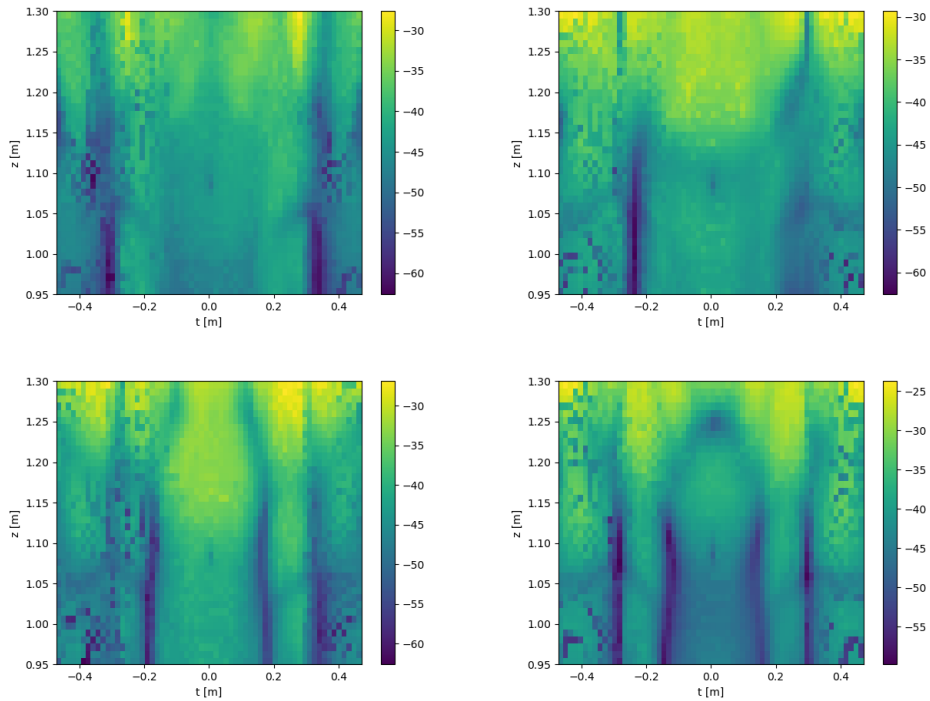


Figure 3.12: Magnitude of the electric field around the body for the fat model in the four chosen locations (the end of the esophagus, in the small bowel, at the beginning of the intestine, and at the end of the intestine) in dB scale

It can therefore be stated that, in the case of a homogeneous fat model, the results obtained do not vary substantially in the four positions analyzed along the GI tract. In fact, the distance values between Tx and Rx and the electric field are

similar to each other. A difference can also be noted between the results obtained for the homogeneous air model. These differences are mainly due to the different permittivity and conductivity that fat has compared to air. Furthermore, there is a less hyperbolic relationship between the recorded distance between Tx and Rx and the electric field.

3.2.2 Comparison between different Rx positions for the fat model

Also in the case of the homogeneous fat model, a study was conducted in which the location within the GI tract did not vary (at the end of the esophagus), while the parameter was the position of Rx. In particular, the electric field and distance between Tx and Rx values were evaluated in all possible configurations of Rx, both internal and external to the body.

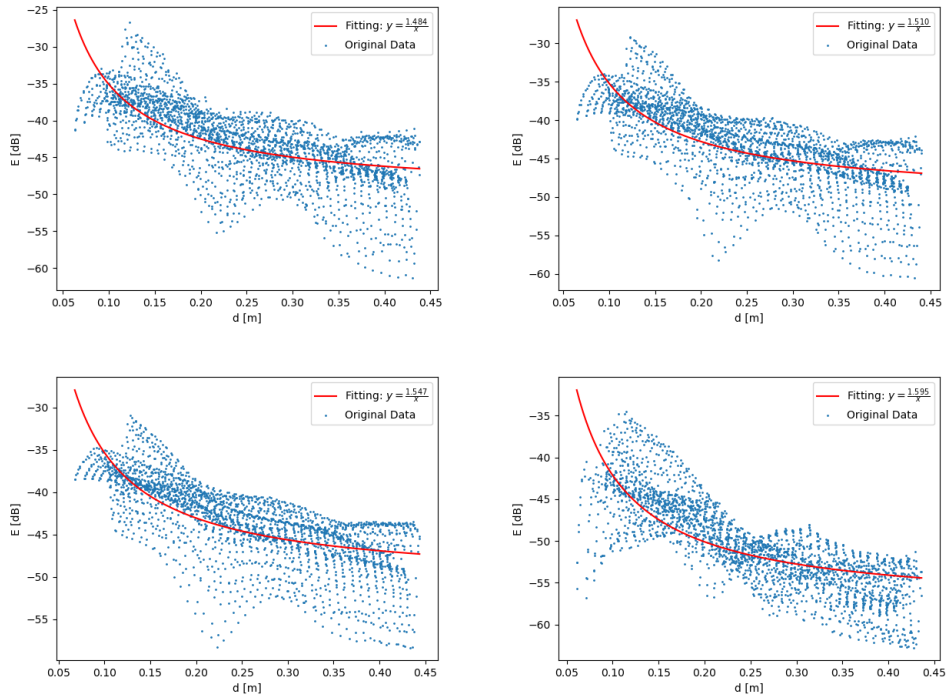


Figure 3.13: Graph of distances between Tx and Rx and electric field for the position 4 mm, 10 mm, 20 mm, and -6 mm of the Rx antenna for the fat model with their interpolation curve

Some examples of graphs obtained have been reported in Figure 3.13, in particular those relating to positions of Rx at 4 mm, 10 mm, 20 mm, and -6 mm.

Furthermore, in this plot it is also possible to observe the hyperbolic interpolation curve with the corresponding equation. The shape of the graph is much more enlarged than that obtained for the air model. In addition, the distances between Tx and Rx are slightly lower than those recorded for the previous model. If different Rx positions are considered, the distance between Tx and Rx values does not fluctuate significantly, as can also be seen from the graphs. The data obtained are slightly different if positive (external to the body) or negative (internal) Rx positions are considered. In fact, the shape that the points take on is different. Furthermore, the electric field ranges obtained are also slightly different. Moreover, for Rx positions equal to 50 mm and 80 mm (both positive and negative) the curves obtained are less similar to those obtained for the other Rx positions.

Rx dis [mm]	Min E [dB]	Max E [dB]	Mean E [dB]	P25 [dB]	P75 [dB]
2	-62.62	-27.62	-43.36	-46.64	-39.36
4	-61.28	-26.70	-42.98	-46.06	-39.34
6	-61.16	-28.02	-42.96	-46.10	-39.42
8	-61.02	-28.64	-43.08	-46.12	-39.58
10	-60.48	-29.20	-43.20	-46.24	-39.72
14	-59.58	-29.86	-43.40	-46.28	-39.994
20	-58.36	-30.92	-43.66	-46.40	-40.24
30	-57.36	-32.34	-43.94	-46.60	-40.72
50	-66.60	-31.90	-58.32	-46.82	-41.48
80	-59.26	-23.70	-44.50	-46.82	-42.12
-2	-64.04	-30.28	-46.20	-50.60	-41.72
-4	-63.56	-34.28	-49.82	-49.82	-45.78
-6	-62.76	-34.50	-51.02	-53.90	-46.46
-8	-62.80	-23.44	-50.18	-53.84	-46.28
-10	-62.94	-23.42	-50.08	-53.76	-46.04
-14	-63.80	-34.46	-49.92	-53.56	-45.88
-20	-64.32	-34.52	-49.84	-53.60	-45.90
-30	-63.92	-36.04	-48.96	-54.12	-45.60
-50	-60.60	-38.60	-48.98	-53.68	-44.20
-80	-74.52	-41.30	-50.54	-55.84	-44.28

Table 3.4: Values of maximum, minimum, mean, 25th percentile, and 75th percentile of the electric field in dB for different Rx positions for the fat model

The electric field values of maximum and minimum and the calculated ones, such as the mean value, the 25th and 75th percentile can be analyzed in Table 3.4. The minimum and maximum values are approximately at all Rx positions varying between -30 dB and -60 dB. For negative Rx positions, they assume slightly lower

values. The same behavior follows the average, 25th and 75th percentile values where it can be noted that for Rx positions outside the body, these parameters are bigger. Furthermore, as previously noted from the plots, the electric field values obtained for the 50 mm and 80 mm positions of Rx, both positive and negative, undergo variations with respect to the other Rx positions. Furthermore, for positions equal to -8 mm and -10 mm the maximum field value is bigger.

For this homogeneous fat model, it can therefore be stated that the results obtained for the different Rx positions tend to be quite similar with minimal variations. The most distant positions, both the internal and external ones, differ in terms of electric field values.

3.3 Muscle model

This section is dedicated to the simulation of the journey of the WCE capsule inside the GI tract for the homogeneous muscle model. It consists of the Duke model, where all the materials of which the model was made of are changed into muscle (Permittivity 47.5 F/m and conductivity 0.57 S/m).

3.3.1 Comparison between different locations inside the GI tract for the muscle model

The first location analyzed is the one at the end of the esophagus. The correspondent plot can be seen in Figure 3.14. The first feature that emerges is the fact that the point cloud is much larger. In fact, if it is compared with the plots obtained for air and fat, it can be seen that there is no direct and easily definable relationship between the distance between Tx and Rx and the electric field.

As regards the range of distance between Tx and Rx values, the minimum is 0.0625 m, while the maximum is 0.4375 m. Furthermore, the mean value is 0.2518 m. It is important to note that these values are in line with those obtained for previous models.

As mentioned previously, since the graph does not have a shape similar to a hyperbola, the R^2 value turns out to be 0.3589. It is lower than that obtained for the other models.

If we move in the small bowel, the results obtained can be examined in Figure 3.15. In fact, it can be seen that the minimum observed distance between Tx and Rx is 0.0397 m and the maximum is 0.4083 m. The calculated average value amounts to 0.2216 m. Also in this case these values do not change substantially compared to the previous ones.

In this particular case, the parameter that changes is R^2 . In fact it is equal to 0.6090. Indeed, it can be seen that the points are in a different shape as those at

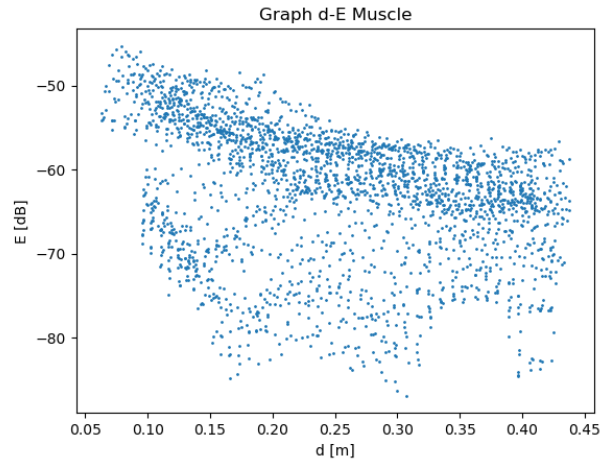


Figure 3.14: Graph of distances between Tx and Rx and electric field for a location at the end of the esophagus for the muscle model

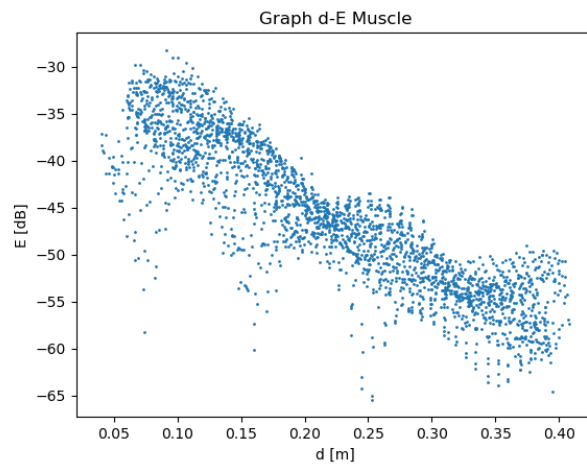


Figure 3.15: Graph of distances between Tx and Rx and electric field for a location in the small bowel for the muscle model

the end of the esophagus for the muscle model.

As regards the beginning of the intestine, the corresponding graph is the Figure 3.16. The minimum in distance between Tx and Rx amounts to 0.0219 m and the maximum to 0.3250 m. The mean value is 0.1950 m. This range and the average value are slightly lower than those previously analyzed for the muscle model in different areas of the GI tract.

Interpolation with a hyperbola is once again difficult due to the presence of a

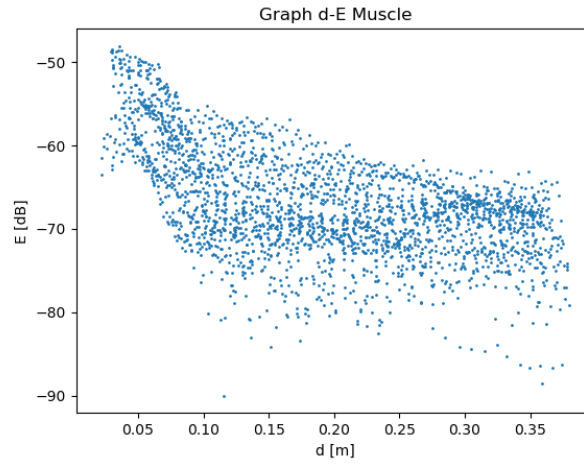


Figure 3.16: Graph of distances between Tx and Rx and electric field for a location at the beginning of the intestine for the muscle model

larger point cloud. In fact, the calculated R^2 value is 0.3250. This value is lower than both that obtained for the end of the esophagus and that in the small bowel.

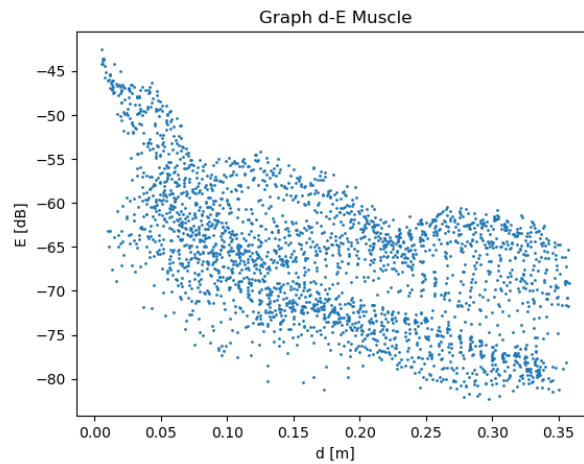


Figure 3.17: Graph of distances between Tx and Rx and electric field for a location at the end of the intestine for the muscle model

The last section analyzed is the one at the end of the intestine (Figure 3.17). In this case, the range of distance between Tx and Rx values extends from a minimum of 0.0052 m to a maximum of 0.3580 m. The mean is 0.1761 m. It can be deduced that these data are the lowest among all the areas analyzed.

The value of R^2 obtained by interpolation with a hyperbola is 0.5238. It can be seen that it is intermediate with respect to that resulting from the analysis at the beginning of the intestine and in the small bowel.

Position	Max E [dB]	Min E [dB]	Mean E [dB]	P25 [dB]	P75 [dB]
1	-45.31	-86.87	-62.54	-67.27	-56.94
2	-28.24	-65.72	-46.14	-52.56	-39.52
3	-48.11	-89.99	-67.01	-71.12	-63.26
4	-42.52	-82.27	-66.26	-72.05	-61.95

Table 3.5: Electric field parameters for the muscle model in the positions illustrated in Figure 3.1

The electric field values obtained in the four Rx positions analyzed can be highlighted in Table 3.5. In particular, it can be seen that the range of values (maximum and minimum) varies quite significantly. Moreover, in the small bowel, the field values are shifted towards higher values. For the other three positions, the range has lower values. Furthermore, at the beginning of the intestine, the calculated values (mean, 25th and 75th percentile) are lower than in the other configurations.

The representation of the electric field with respect to a planar section for the muscle model can be found in the Figure 3.18. It can be seen how in the first two positions analysed, the field assumes bigger values in the upper part, while it decreases in the lower part, non-linearly. Furthermore, for the beginning of the intestine, the center-left area is characterized by a smaller field, while medium-high values can be seen in the rest of the plan. Field representation in the end of the intestine shows a top-down decrease from high to low values.

In the case of the homogeneous muscle model there are quite significant variations when considering different points within the GI tract. In fact, the point at the beginning of the intestine is different from the others. For this point, smaller electric field values and different calculated parameters were recorded compared to the other positions. The homogeneous muscle model, in fact, has a higher permittivity and conductivity. This affects the results obtained.

3.3.2 Comparison between different Rx positions for the muscle model

An analysis of the results obtained in the area at the end of the esophagus by varying the position of the Rx was conducted, as well as for the homogeneous muscle model. In particular, both negative and positive positions have been observed.

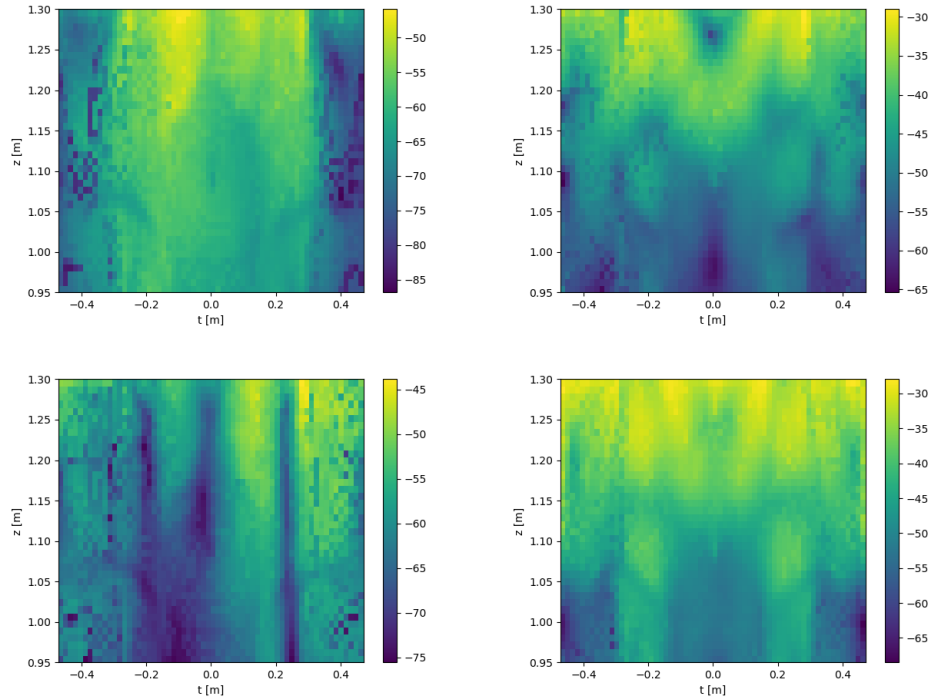


Figure 3.18: Magnitude of the electric field around the body for the muscle model in the four chosen locations (the end of the esophagus, in the small bowel, at the beginning of the intestine and at the end of the intestine) in dB scale

In Figure 3.19, there are some examples of positions of Rx equal to 4 mm, 10 mm, 20 mm, and -6 mm in terms of Tx and Rx distance and electric field. In addition, there is the hyperbolic interpolation curve with its equation. Compared to previous models, the muscle provides a denser upper point cloud that is quite distinct from the lower one. An analysis was conducted in order to understand whether this division could be caused by the succession of points ordered above or below or if there were other reasons. Unfortunately, no satisfactory explanation has been found to explain this phenomenon. Surely it is clearly noted that the results obtained in the plot do not come particularly close to a hyperbole. In fact, an orderly decrease of the electric field cannot be deduced as the distance between Tx and Rx increases.

In Table 3.6, the maximum and minimum values of the electric field for the muscle model and the respective calculated parameters are visible. It can be immediately seen how the electric field range has shifted towards lower values compared to the previous models analyzed. In particular, it can also be underlined that for Rx positions inside the body, the maximum and minimum of the electric

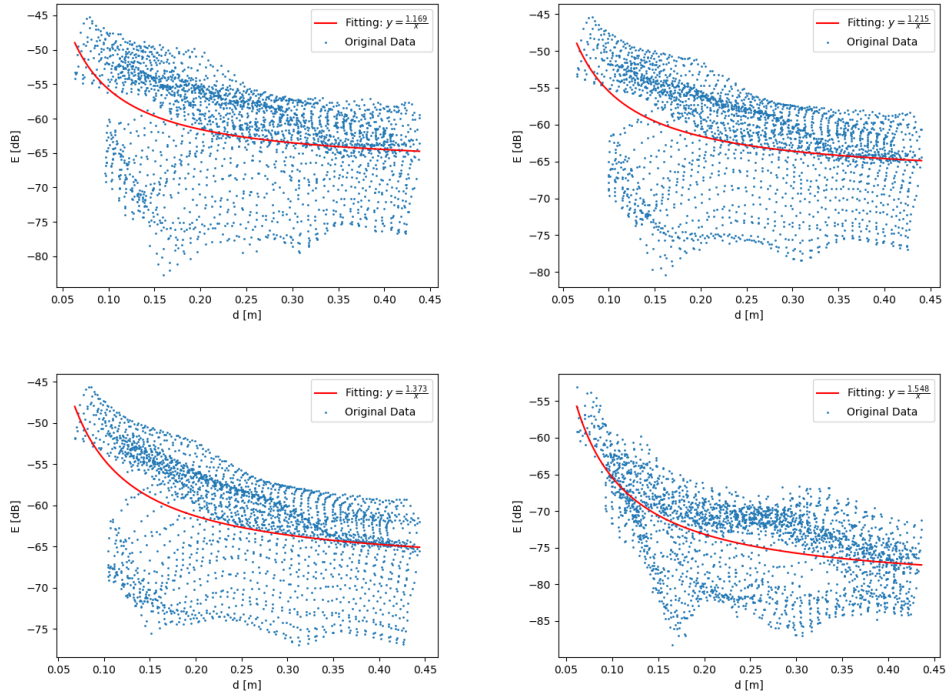


Figure 3.19: Graph of distances between Tx and Rx and electric field for the position 4 mm, 10 mm, 20 mm, and -6 mm of the Rx antenna for the muscle model with their interpolation curve

field are lower than for external positions. Consequently, the mean, 25th and 75th percentile parameters also follow the same trend. Furthermore, it can also be seen that there is a difference between the electric field values obtained for external positions of Rx versus internal positions. Indeed, for negative values of Rx, the electric field assumes a smaller range than for positive values of Rx. Consequently, the calculated electric field parameters (mean, P25, and P75) also have the same tendency.

Likewise in the homogeneous fat model, different behaviour between internal and external Rx positions was recorded for the muscle model. Furthermore, the position of the WCE along the GI tract also plays a key role in the results obtained.

3.4 Duke model

This section is dedicated to the stimulation of the journey of the WCE capsule inside the GI tract with the heterogeneous Duke model. It consists of the complete model, where all the materials from which the model was made are considered. It

Rx dis [mm]	Min E [dB]	Max E [dB]	Mean E [dB]	P25 [dB]	P75 [dB]
2	-86.87	-45.31	-62.54	-67.27	-56.94
4	-82.66	-45.22	-61.82	-65.26	-56.82
6	-81.94	-45.32	-61.86	-65.90	-57.28
8	-80.80	-45.38	-61.90	-65.96	-57.04
10	-80.36	-45.40	-61.92	-65.98	-57.12
14	-78.60	-45.52	-61.90	-65.98	-57.18
20	-69.00	-45.64	-61.82	-65.92	-57.26
30	-74.42	-45.42	-60.98	-65.40	-57.06
50	-66.60	-50.90	-58.32	-46.82	-41.48
80	-72.60	-44.54	-60.00	-65.10	-56.34
-2	-87.76	-45.44	-66.90	-74.92	-59.46
-4	-88.68	-51.20	-72.40	-77.52	-68.40
-6	-88.22	-53.08	-73.36	-77.70	-69.70
-8	-88.18	-51.42	-73.80	-78.48	-70.14
-10	-88.90	-52.94	-74.26	-79.00	-70.58
-14	-90.78	-54.18	-72.92	-79.82	-71.16
-20	-95.16	-56.58	-75.92	-80.92	-71.68
-30	-97.44	-58.64	-77.16	-82.66	-73.12
-50	-99.76	-60.10	-78.00	-84.66	-74.84
-80	-96.24	-65.84	-82.30	-86.76	-76.14

Table 3.6: Values of maximum, minimum, mean, 25th percentile, and 75th percentile of the electric field in dB for different Rx positions for the muscle model

is the most complex simulation among those analyzed.

3.4.1 Comparison between different locations inside the GI tract for the Duke model

The analysis conducted for the complete heterogeneous Duke model started, as in the previous cases, from the point at the end of the esophagus (Figure 3.20). The minimum distance between Tx and Rx recorded was 0.0052 m, while the maximum was 0.4421 m. The average of the points obtained is 0.1759 m. It can be seen that these results are among the lowest reported.

At first glance, it is clear that this graph is nowhere near that of a hyperbola. In fact, his interpolation with this curve generated an R² equal to 0.0949. This value supports the idea that there is no hyperbolic relationship between distance and electric field for this heterogeneous model.

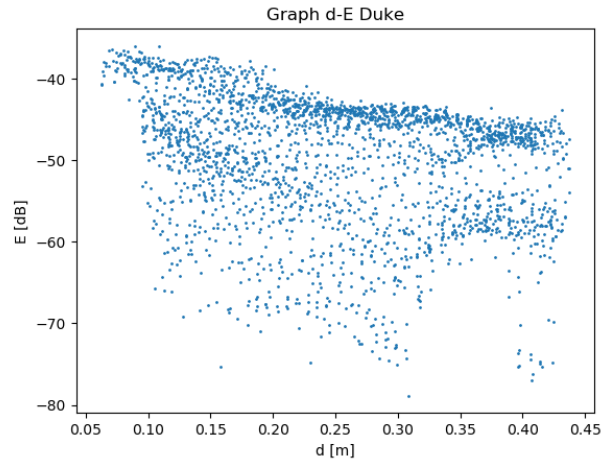


Figure 3.20: Graph of distances between Tx and Rx and electric field for a location at the end of the esophagus for the Duke model

If the analysis is moved to the small bowel, the results obtained are not particularly divergent from those obtained at the end of the esophagus for the complete Duke model. The results can be seen in Figure 3.20. Indeed, the range for the distances between Tx and Rx extends between 0.0056 m and 0.4335 m. The average value amounts to 0.1760 m.

Again the shape of the curve is not similar to a hyperbola. Thus, the calculated R^2 value for this type of interpolation is 0.1540.

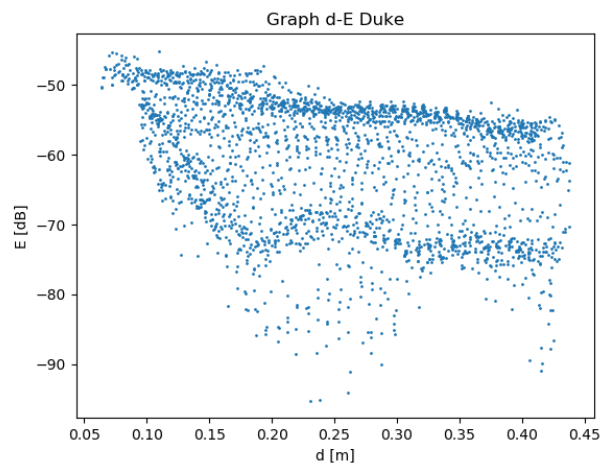


Figure 3.21: Graph of distances between Tx and Rx and electric field for a location in the small bowel for the Duke model

As far as the beginning of the intestine is concerned, the minimum distance between Rx and Tx value recorded is 0.0050 m, while the maximum value is 0.4433 m as it can be seen in Figure 3.22. The average of the data obtained is 0.1758 m. Therefore, there are no particular variations in this case either, compared to the previous points.

The value of R^2 for interpolation with a hyperbola is 0.2286. It is slightly higher than the previous ones. Despite this, the curve is not comparable to a hyperbola.

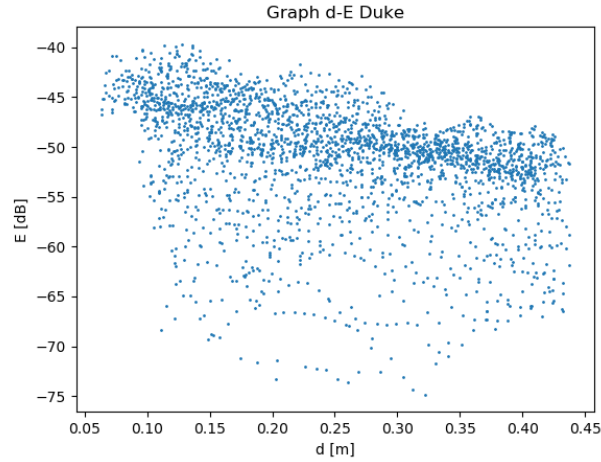


Figure 3.22: Graph of distances between Tx and Rx and electric field for a location at the beginning of the intestine for the Duke model

The last location analyzed is the one at the end of the intestine. The results are visible in the Figure 3.23. The range of distance between Tx and Rx extends between the minimum 0.0057 m and the maximum 0.4312 m. The resulting mean of the data is 0.1760 m. Even this latest study for the complete Duke model did not lead to substantial variations in terms of distances.

Instead, the curve is more compact than the previous plots. Therefore the value of R^2 in this case is 0.4096. Obviously, the curve does not look like a hyperbola, but it is closer than the other points analyzed.

In Table 3.7, the electric field values recorded at the four locations within the GI tract for the complete Duke model can be observed. A certain variability can be highlighted both in terms of the range and of the parameters calculated. In particular, the electric field in the small bowel assumes much lower values than in the other areas analyzed. Instead, in the final part of the intestine the field is higher. The other two positions assume intermediate values. In general, the ranges are slightly lower than in the previous models analyzed.

As for the electric field on a planar surface for the complete Duke model, it can be analyzed in Figure 3.24. It can be stated that in the first two positions,

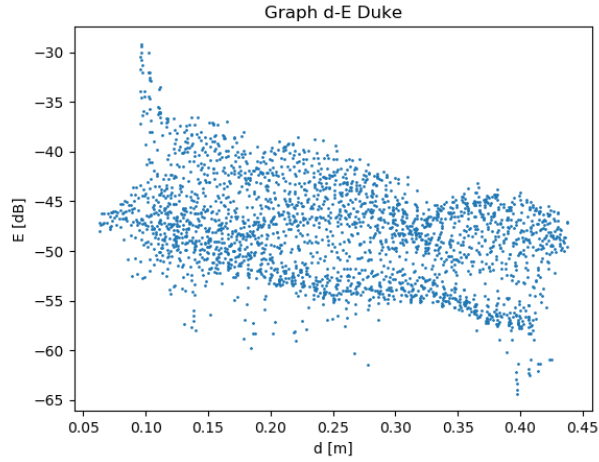


Figure 3.23: Graph of distances between Tx and Rx and electric field for a location at the end of the intestine for the Duke model

Position	Max E [dB]	Min E [dB]	Mean E [dB]	P25 [dB]	P75 [dB]
1	-36.04	-78.86	-48.76	-55.08	-44.08
2	-45.18	-95.22	-61.10	-69.22	-53.80
3	-39.72	-72.84	-51.00	-53.14	-47.18
4	-29.20	-64.38	-48.14	-51.64	-45.26

Table 3.7: Electric field parameters for the Duke model in the positions illustrated in Figure 3.1

the electric field in the central part assumes greater values, while in the lateral part, it is lower. For the representation of the beginning of the intestine, the field varies if one moves horizontally from areas with high values to others with low quantities. In the area of the end of the intestine, the presence of a central area with a medium-high field surrounded by a part with an even higher field can be noted.

It can therefore be concluded that the results obtained for the different positions of the WCE along the GI tract are different between each other for the heterogeneous model. In fact, the electric field range and the calculated parameters vary depending on the position of the WCE. This behaviour is due to the nature of the human body. In fact, as the heterogeneous Duke model represents, it is formed by the combination of several tissues, each with different conductivity and permittivity. These tissues are present at different locations in the GI tract in different sequences and percentage. This is why the electric field at the various points is different.

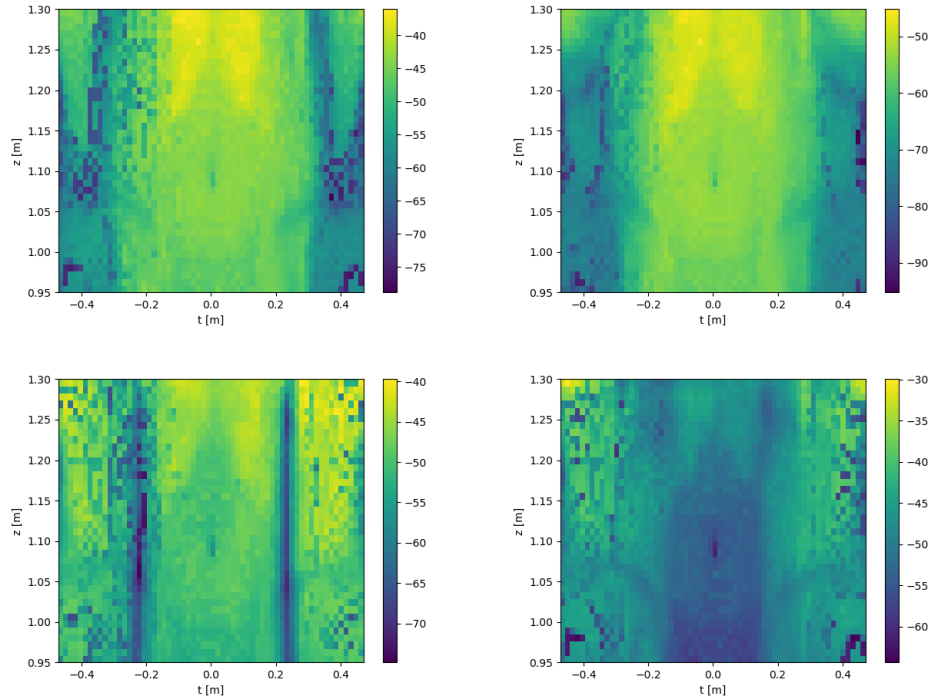


Figure 3.24: Magnitude of the electric field around the body for the Duke model in the four chosen locations (the end of the esophagus, in the small bowel, at the beginning of the intestine, and at the end of the intestine) in dB scale

3.4.2 Comparison between different Rx positions for the Duke model

The goal of this section is to analyze the relationship between different Rx positions, holding the location constant within the GI tract (end of the esophagus) for the full Duke model.

In Figure 3.25 it can be found some examples of graphs in which the distance between Tx and Rx and the electric field are related. In particular, the positions of Rx represented are 4 mm, 10 mm, 20 mm, and -6 mm. Moreover, a hyperbolic interpolation with the related equation has been shown. As with the muscle model, the shape of the curve cannot be defined through a hyperbolic relationship. In fact, it can be seen that for each position of Rx, can be talked about a cloud of points and the interpolation is not representative of the results obtained. For Rx positions inside the body, it can be said that there is even less relationship than the one for positive positions.

Table 3.8 shows the maximum and minimum values of the electric field, the mean, and the 25th and 75th percentiles for the complete Duke model. An important

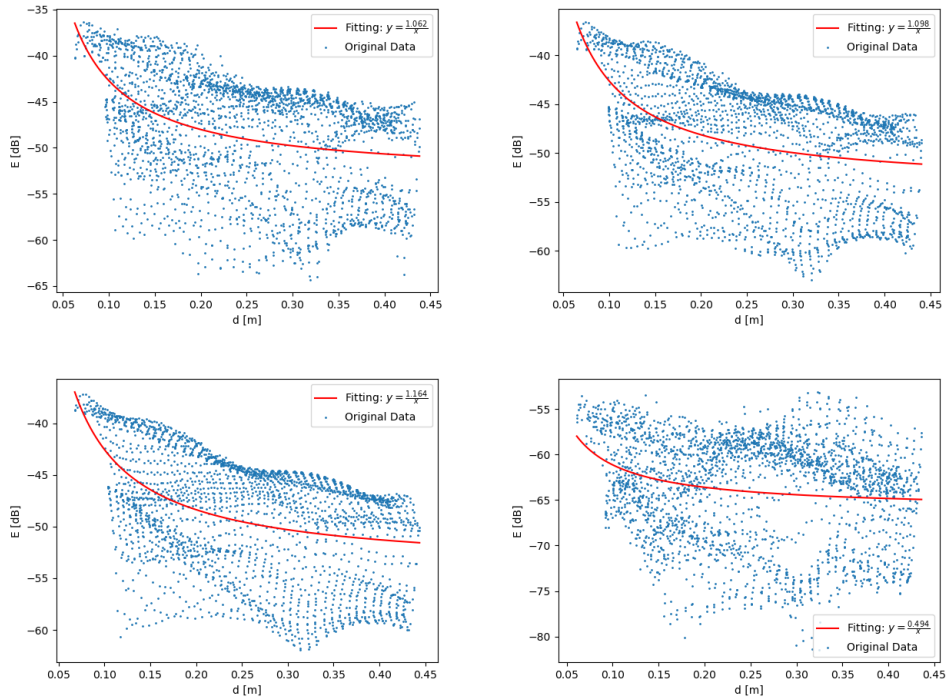


Figure 3.25: Graph of distances between Tx and Rx and electric field for the position 4 mm, 10 mm, 20 mm, and -6 mm of the Rx antenna for the Duke model with their interpolation curve

difference in range between positive and negative positions of Rx can be immediately noticed. In particular, lower values are present for internal positions of the body, while for external ones the electric field assumes higher values. This trend can also be seen from the calculated parameters. In fact, both the mean and the 25th and 75th percentiles are greater for positive Rx distances and smaller for negative.

It can therefore be stated that even if the heterogeneous model case is considered, the position of Rx leads to significantly different electric field values. This is because the distance between Tx and Rx varies depending on whether the receivers are inside or outside the human body.

3.5 Models comparison

In this section, a comparison among the different models analyzed has been performed. In particular, in terms of different ranges of values of electric field and hyperbolic interpolation, normalization with the different input power and different electric field distribution around the Tx antenna.

Rx dis [mm]	Min E [dB]	Max E [dB]	Mean E [dB]	P25 [dB]	P75 [dB]
2	-78.86	-36.04	-48.76	-55.08	-44.08
4	-64.28	-36.36	-48.24	-52.48	-44.12
6	-63.74	-36.46	-48.30	-52.42	-44.24
8	-62.96	-36.52	-48.36	-52.44	-44.34
10	-62.92	-36.62	-48.44	-52.50	-44.46
14	-62.36	-36.74	-48.58	-52.58	-44.46
20	-61.90	-37.18	-48.82	-53.26	-44.96
30	-61.52	-37.58	-49.16	-52.84	-45.42
50	-66.60	-50.90	-58.32	-46.82	-41.48
80	-60.96	-38.16	-49.70	-53.12	-46.16
-2	-85.56	-35.98	-55.70	-64.48	-45.90
-4	-88.12	-40.54	-62.50	-67.48	-58.36
-6	-81.46	-53.10	-63.66	-66.46	-59.16
-8	-87.36	-51.38	-64.18	-68.38	-79.48
-10	-87.22	-51.26	-64.86	-68.86	-60.16
-14	-84.58	-52.02	-65.78	-69.82	-61.06
-20	-88.58	-53.96	-66.88	-72.04	-61.98
-30	-89.52	-53.78	-68.28	-72.84	-63.48
-50	-97.30	-54.70	-71.88	-75.60	-67.38
-80	-89.52	-63.40	-76.266	-78.60	-73.30

Table 3.8: Values of maximum, minimum, mean, 25th percentile and 75th percentile of the electric field in dB for different Rx positions for the Duke model

3.5.1 Interpolation values

It is important to analyze how, for the different models, the electric field and distance results between Tx and Rx can be compared. In this regard, Figure 3.26 shows the results obtained for each model in the position at the end of the esophagus for a position of Rx of 2 mm outside the body.

It appears immediate how the air model, compared to the others, is the one with more compact values and more similar to a hyperbolic curve. The other models, on the other hand, are formed by a scattering of points. It can be seen that the highest electric field values are those for the fat model (as can also be seen from Table 3.4 in the previous section), while the lowest are those for the muscle model. The models analyzed, therefore, when compared in terms of the electric field, show different values due to the nature of the tissue analyzed, and their conductivity and permittivity.

Moreover, it was evaluated how much the electric field and distance values

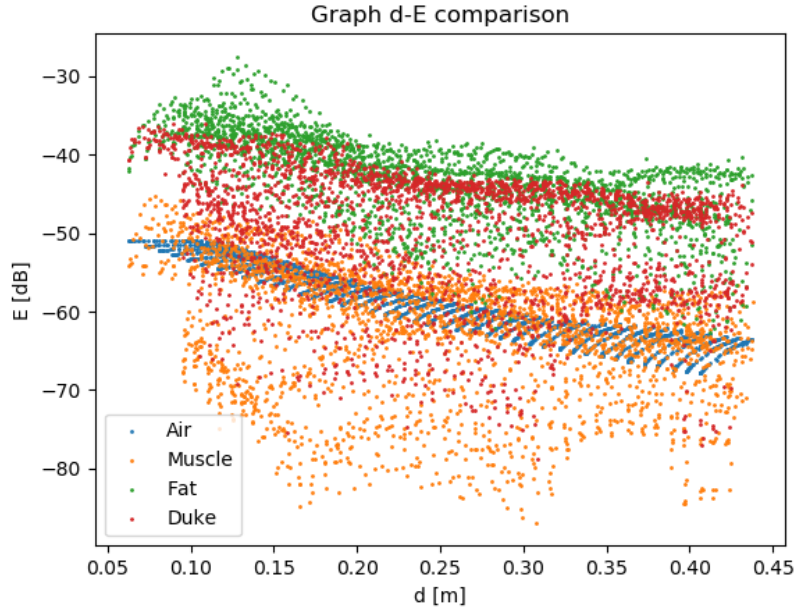


Figure 3.26: Comparison between the four models

between Tx and Rx are interpolable with a hyperbolic curve. The GI tract point was kept constant and at the end of the esophagus. The analysis was done in terms of R^2 . In the Table 3.9 it can be found the various values of R^2 divided by each model and by all the Rx positions.

It can be seen that for each model, the range of R^2 is very different. In fact, the highest values are those obtained for the air model, as they are the closest to hyperbolic interpolation. The second most similar to this curve are those of the fat model. They are slightly lower than those of air but in any case the value of R^2 is medium-high. On the other hand, the results obtained for the muscle and for the heterogeneous complete Duke model are lower. In fact, the latter has very low values. For this reason, the relationship between the electric field and the distance between Tx and Rx is not hyperbolic in this case.

Furthermore, it can be noted that, for all models, there is a drop in the R^2 parameter when one passes from positive values of Rx to negative values. This means that for positive values of Rx there is a greater resemblance to hyperbolic interpolation.

Rx dis [mm]	R ² air	R ² fat	R ² muscle	R ² Duke
2	0.7725	0.6247	0.3250	0.0949
4	0.7731	0.6540	0.3754	0.1610
6	0.7742	0.6565	0.3856	0.1689
8	0.7749	0.6587	0.3936	0.1892
10	0.7757	0.6595	0.4001	0.1890
14	0.7773	0.6629	0.4112	0.2018
20	0.7803	0.6708	0.4256	0.2242
30	0.7812	0.6805	0.4427	0.2380
50	0.7866	0.6994	0.4769	0.2836
80	0.7878	0.7054	0.5062	0.3083
-2	0.7714	0.6118	0.1363	0.0132
-4	0.7704	0.6653	0.1163	0.0162
-6	0.7694	0.6912	0.1308	0.0141
-8	0.7682	0.6960	0.1408	0.0021
-10	0.7671	0.6991	0.1599	0.0001
-14	0.7604	0.7006	0.1799	0.0002
-20	0.7381	0.6722	0.1957	0.0003
-30	0.7811	0.6297	0.1814	0.0017
-50	0.6700	0.5846	0.0939	0.0468
-80	0.6285	0.5638	0.0021	0.0001

Table 3.9: Values of R² for hyperbolic interpolation

3.5.2 Input powers

It was important to consider the input power of the Tx antenna because, if you want to compare the electric field values obtained for the different models, this parameter plays a fundamental role. Actually, the Tx input power can change, depending on the type of tissue surrounding the antenna. In fact, previous studies conducted on this antenna showed that its behavior is similar to a capacitor. This can be seen as the power results obtained have a large imaginary part compared to the real one. This is also a symptom of antenna inefficiency. This choice, on the other hand, was made to have a small antenna that could enter the capsule. In this way, the real part of the collected power has been entered in Table 3.10.

The conductivity and permittivity properties of the antenna in the Tx sphere are more similar to those of fat and muscle. For this reason, the input power obtained assumes a larger value in these cases. As for the air model, it has the most different properties than the antenna. Therefore, it will have a much lower input power value, thus resulting in worse behavior. As for Duke's complete model, its input

Model	Input Power [W]
Air	3.0×10^{-8}
Fat	3.6×10^{-5}
Muscle	1.2×10^{-4}
Duke	1.1×10^{-4}

Table 3.10: Real part of the input power of the Tx antenna for the different body models

power value is the combination of the interaction of the antenna with the properties of various tissues whose the model is made of. This results in a value very similar to the one for the muscle model. In conclusion, the recorded input power values are quite low. These therefore reveal a not too high antenna efficiency.

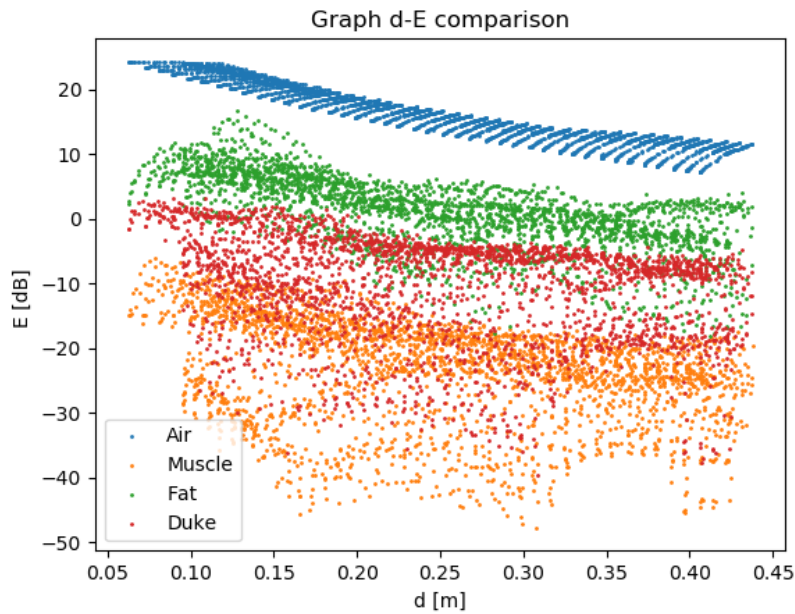


Figure 3.27: Comparison between the four models normalized by the input power in dB scale

Subsequently, for the analysis, the point at the end of the esophagus was chosen, at a Rx distance of 2 mm external to the body and orientation along the vertical axis of the body (z-axis). For each of the models analyzed, the square root of the input power value was calculated. Then, each electric field value was divided by this last value distinctive for the different models. In this way, it was possible to

compare the results, without having the Tx input power bias. The results obtained are in the Figure 3.27. It can be seen how the values of the air model, which without this normalization were among the lowest (Figure 3.26), are now the highest. As for the other three models, since they have a similar input power, their relative position in the graph does not vary much. It can therefore be said that input power plays a fundamental role in the results obtained.

3.5.3 Tx antenna electric field propagation

It is very important to analyze how the electric field propagates in the various tissues of the human body in order to understand how this parameter influences the results obtained for the different models. In particular, sections on the XY plane were evaluated where the electric field value is maximized. This point is around the location of the Tx antenna. The data obtained refer to a location at the end of the esophagus. Furthermore, the values were normalized with respect to the maximum RMS value of the electric field obtained. For each of the four simulated models, three orientations of the Tx antenna were taken into consideration:

- Oriented towards the x-axis;
- Oriented towards the y-axis;
- Oriented towards the z-axis.

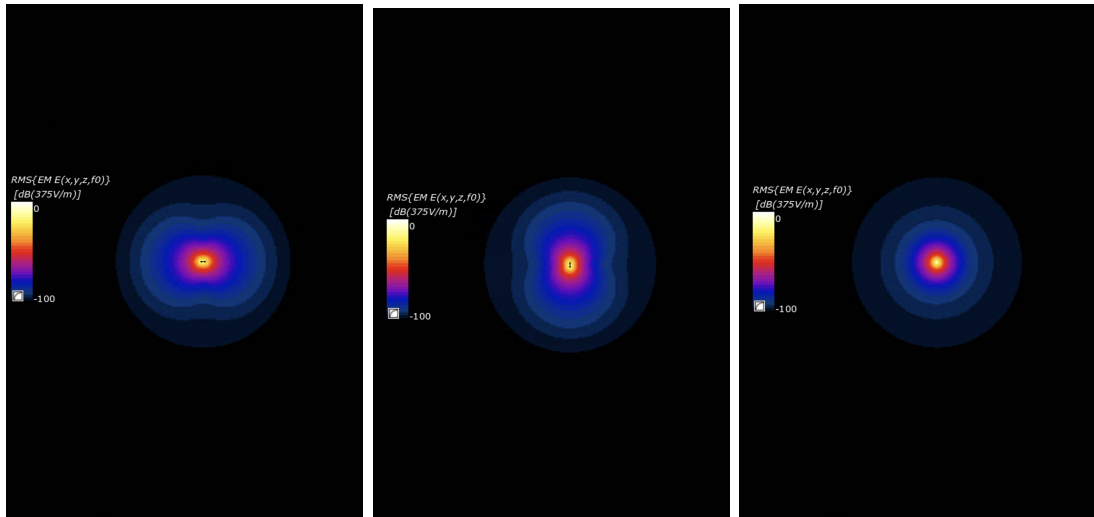


Figure 3.28: XY plane representation of the electric field through the Tx antenna orientated toward x, y, and z for the air model

As regards the results obtained for the homogeneous model made up of air, they can be observed in the Figure 3.28. In particular, it can be seen how the electric field around the Tx antenna follows an almost regular pattern. In fact, moving away from the antenna there are concentric circular crowns that contain similar electric fields. They have decreasing electric field values as they move away from the center. It can be observed that when the Tx antenna is oriented parallel to the z axis, the electric field circles are almost perfect, while when it is oriented in the x and y direction the surfaces are not perfectly circular. This is due to the fact that when the antenna is oriented towards the z axis it is parallel to the vertical body axis.

These results are what one might expect from a homogeneous air model. Indeed, the antenna with orientation parallel to the z-axis radiates almost in perfect circles. This means that there is a 1:1 relationship in this orientation. In the other two orientations, there will be losses due to the difference in elevation angle of the Tx antenna.

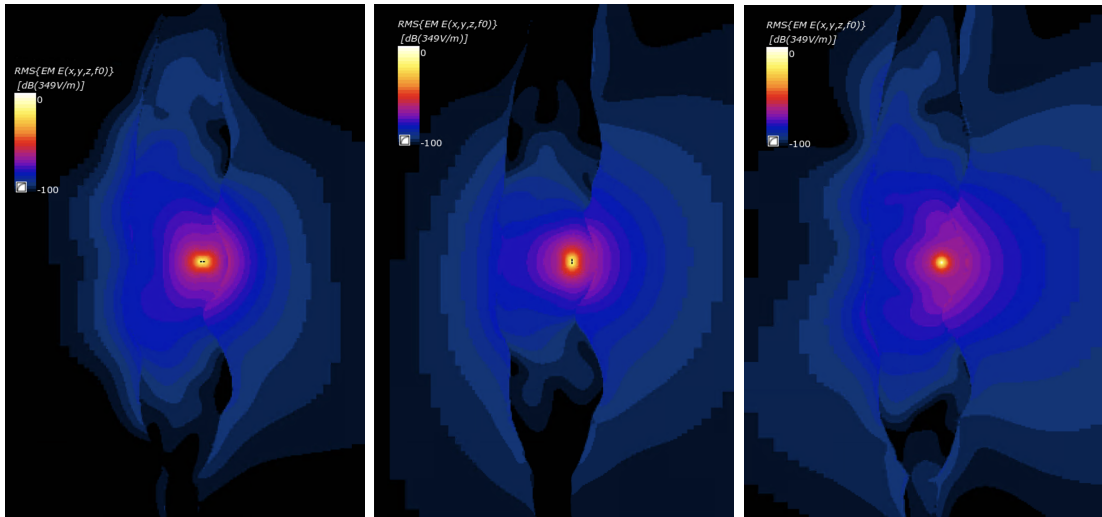


Figure 3.29: XY plane representation of the electric field through the Tx antenna orientated toward x, y and z for the fat model

The results obtained for the homogeneous fat model are visible in the Figure 3.29. In particular, unlike the air model (Figure 3.28), the electric field does not decrease with concentric circles around the antenna. In fact for this second model the pattern of decrement of the field is not regular. Also, the normalization value for this model is smaller than the previous one. In the Figure 3.29 it can clearly be seen that the area around the antenna is developed more in space in one direction. Furthermore, the electric field decreased more slowly. This can be seen by the larger size of the blue area. For the fat model, due to the fact that at the interface

between the antenna and the model there is a lot of difference in permittivity and conductivity, this different shape has been registered. This creates the irregular effect of decreasing the electric field.

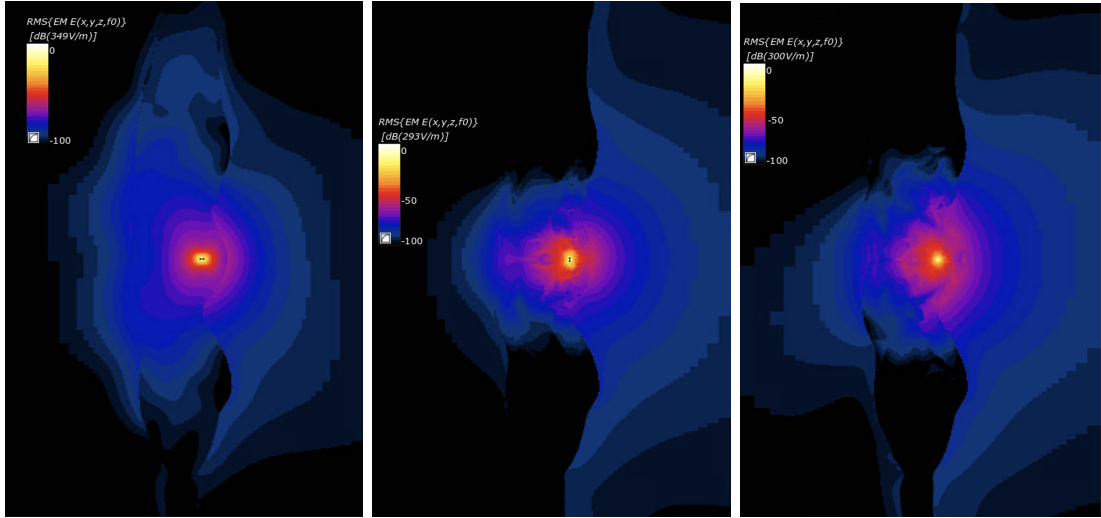


Figure 3.30: XY plane representation of the electric field through the Tx antenna orientated toward x, y, and z for the muscle model

The muscle model brought the results visible in Figure 3.30. In this case, the normalization value is the lowest among the models considered. As with the fat model, the electric field decay around the Tx antenna does not follow a regular pattern. On the contrary, for all three orientations, a zone can be seen, with a shape more developed in one direction, around the Tx antenna where the electric field is bigger. Moving away from the antenna there will be a fairly large area where the electric field is minimal. This type of decrease is mainly due to the properties of the muscle tissue. Indeed, having quite high permittivity and conductivity values, will cause a non-linear decrease of the electric field around the Tx antenna.

The results obtained for the Duke heterogeneous model are visible in Figure 3.31. The normalization value is equal to that for the homogeneous model of muscle and therefore lower than that of fat and air. In this model, the decrease in the electric field is even less regular. In fact, in all three orientations, a small area can be seen in which the electric field is maximum. Moving away from the Tx antenna this parameter decreases in value irregularly and more in one direction than the other. Furthermore, the area where the electric field is smaller is much more directional than in homogeneous models. This phenomenon is given by the complexity of the Duke model which contains all the tissues within it.

In conclusion, the orientation of the WCE plays a fundamental role in the propagation of the electric field. Furthermore, for the different homogeneous

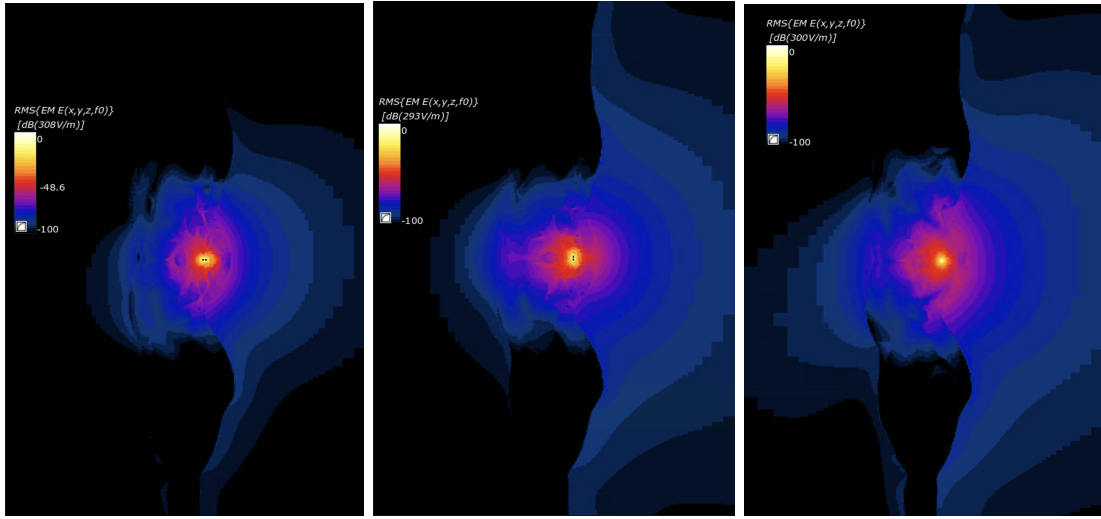


Figure 3.31: XY plane representation of the electric field through the Tx antenna orientated toward x, y, and z for the Duke model

models, the decrease of the electric field around the Tx antenna assumes a different form given by the conductivity and permittivity properties of the fabric model itself. For the Duke heterogeneous model, the decrease will be even more complex as it must take into account all the surrounding tissues.

3.6 Localization error analysis

In this section, an analysis of the error in the localization of the WCE has been performed. In particular, for each of the models considered (air, fat, muscle, and complete Duke) the results obtained for an Rx position of 2 mm external with respect to the body surface and orientation of the WCE parallel to the vertical axis of the body (z-axis) were analyzed. In addition, all four locations within the GI tract shown in Figure 3.1 were considered. Furthermore, all obtained electric field values and distances between Tx and Rx were interpolated with a hyperbolic curve that can be seen in Figure 3.32.

For each of the four models, fixed points of distance between Tx and Rx equal to 0.1, 0.2 and 0.3 m were chosen. Subsequently, in these points, with the hyperbolic interpolation curve visible in the Figure 3.32, the corresponding electric field values were calculated. Subsequently an interval of 1 mV/m was chosen (0.5 mV/m positive and 0.05 mV/m negative) and the maximum, minimum, range, 25th and 75th percentile distance between Tx and Rx in this interval were evaluated taking into consideration all the points obtained.

In Table 3.11 there can be found the results obtained for the air model. It can

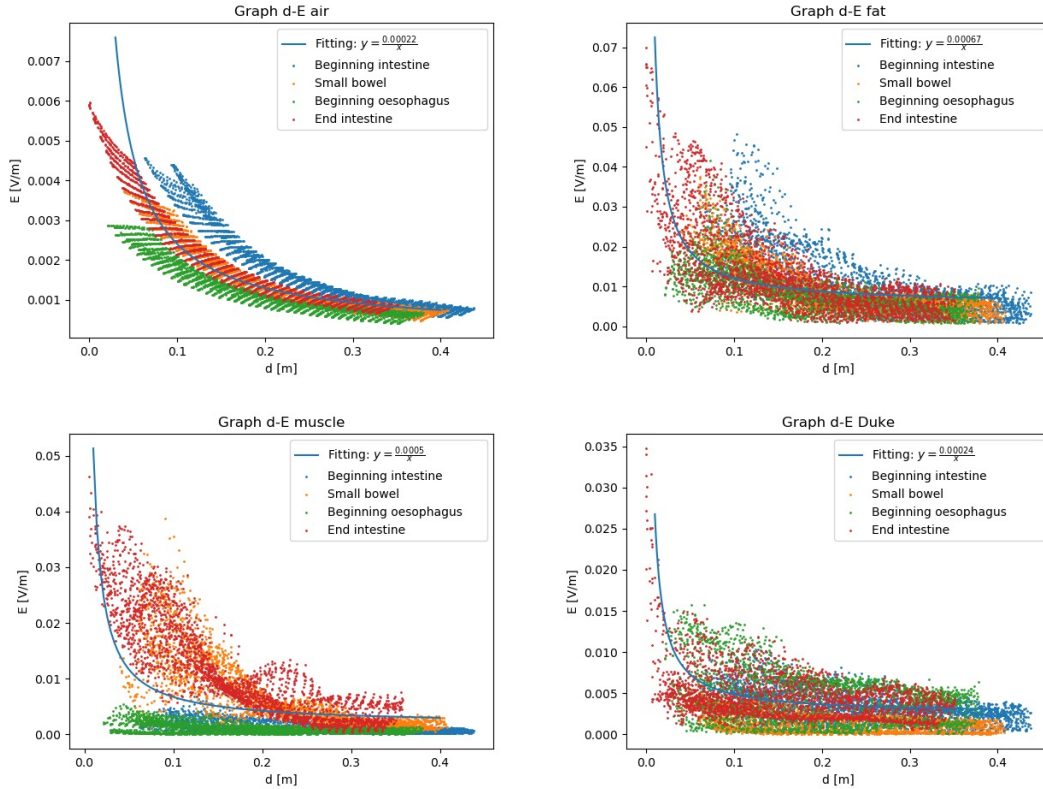


Figure 3.32: Graph of distances and electric field for the four models for localization purposes and their hyperbole interpolation

d[m]	E[mV/m]	Max d[m]	min d[m]	Range[m]	P25[m]	P75[m]	RangeP[m]
0.1	2.406	0.261	0.021	0.240	0.095	0.166	0.071
0.2	1.293	0.438	0.054	0.383	0.177	0.313	0.136
0.3	0.921	0.438	0.071	0.366	0.196	0.320	0.124

Table 3.11: Values of maximum, minimum, range, 25th percentile, 75th percentile, and range P75-P25 of the distances [m] given an electric field [mV/m] calculated with the interpolation curve for the air model

be seen that the maximum distance between Tx and Rx range obtained is 38.3 cm for an electric field value of 1.293 mV/m. Instead, the smallest range is equal to 24.0 cm for a field of 2.406 mV/m. It can therefore be underlined that there is a variability in the range of distances that varies from 24 to 38.3 cm, which are quite different from each other. Also significant is the range P, derived from the difference between the value obtained for the 75th percentile minus the 25th

percentile. For this homogeneous air model, this parameter lies between 16 cm and 18 cm.

d[m]	E[mV/m]	Max d[m]	min d[m]	Range[m]	P25[m]	P75[m]	RangeP[m]
0.1	12.099	0.317	0.025	0.292	0.089	0.182	0.093
0.2	8.744	0.437	0.021	0.416	0.155	0.312	0.157
0.3	7.625	0.436	0.020	0.416	0.176	0.330	0.154

Table 3.12: Values of maximum, minimum, range, 25th percentile, 75th percentile and range P75-P25 of the distances [m] given an electric field [mV/m] calculated with the interpolation curve for the fat model

As for the fat model, the analysis can be done from Table 3.12. Firstly, the electric field values obtained from the interpolation curve are quite different in terms of magnitude compared to those obtained for the air model and very different from each other. In fact, for a distance between Tx and Rx of 0.1 m, the field value obtained is 12.099 mV/m, while for 0.3 m the corresponding value is 7.625 mV/m. Furthermore, the range of distances has a minimum of 29.2 cm for a chosen distance of 0.1 m and a maximum of 41.6 cm for both a distance of 0.2 m and 0.3 m. For this model, the percentile values are not very representative of the corrected distance.

d[m]	E[mV/m]	Max d[m]	min d[m]	Range[m]	P25[m]	P75[m]	RangeP[m]
0.1	6.730	0.358	0.049	0.309	0.171	0.240	0.069
0.2	4.254	0.398	0.032	0.366	0.166	0.252	0.086
0.3	3.429	0.404	0.026	0.378	0.144	0.276	0.132

Table 3.13: Values of maximum, minimum, range, 25th percentile, 75th percentile, and range P75-P25 of the distances [m] given an electric field [mV/m] calculated with the interpolation curve for the muscle model

The results obtained for the muscle model are visible in Table 3.13. The electric field values collected with the interpolating curve for the fixed distances of 0.1, 0.2, and 0.3 m are lower than those of the fat model but higher than those of the air. Furthermore, the range of distances obtained moves from 24 cm for a field of 2.406 mV/m to 36.6 cm for a field equal to 0.921 mV/m. Furthermore, the 25th percentile is quite in line with the distance values for the first two cases considered but not for the third. However, the 75th percentile is higher.

The last model considered is that of complete Duke and the results obtained are represented in Table 3.14. The electric field values obtained in this case in the considered distances between Tx and Rx are not very distant from each other. In

d[m]	E[mV/m]	Max d[m]	min d[m]	Range[m]	P25[m]	P75[m]	RangeP[m]
0.1	4.892	0.410	0.006	0.403	0.115	0.276	0.161
0.2	3.678	0.434	0.006	0.427	0.115	0.301	0.186
0.3	3.273	0.437	0.007	0.430	0.121	0.306	0.185

Table 3.14: Values of maximum, minimum, range, 25th percentile, 75th percentile, and range P75-P25 of the distances [m] given an electric field [mV/m] calculated with the interpolation curve for the Duke model

fact, it can be seen in Figure 3.32 that the interpolation of the Duke model with a hyperbola in the area between 0.1 m and 0.3 m descends slowly. In addition, the range of values obtained for the distances is very high (around 40 cm) for all the considered cases. Furthermore, the calculated percentile values, both the 25th and 75th, are not representative of the true distance between Rx and Tx.

If one wants to compare the range of distances and the range between P75 and P25, it can be seen that for localization, the heterogeneous Duke model presents the largest errors. The lowest values are obtained for the homogeneous air model, followed by the fat model and then the muscle model.

Model	Range [cm]	RangeP [cm]
Air	24.0 - 38.3	7.1-13.6
Fat	29.2 - 41.6	9.3-15.7
Muscle	30.9 - 37.8	6.9-13.2
Duke	40.3 - 43.3	16.1-18.6

Table 3.15: Range of error in distance and range between P75 and P25 for each body model

The summary results of the obtained WCE localization can be found in Table 3.15. In particular, for each simulated model, there are the ranges in terms of maximum and minimum and the difference between the 75th percentile and the 25th percentile in terms of distances in cm given an electric field interpolated with a hyperbolic curve. Although the electric field range within which the distance ranges between Tx and Rx have been calculated is only 1 mV/m, the possible distance ranges are quite high. In particular, it can be noted at first glance that both for the maximum minimum range and for that relating to the percentiles, the largest ranges are those relating to the Duke heterogeneous model. In fact, this result is in line with what we expected since the complexity of the model makes it very difficult to localize the WCE. If the respective range values are evaluated at the maximum and minimum of the distance between Tx and Rx recorded, relative to homogeneous models, the

greatest uncertainty is that for muscle, followed by fat, and finally by air. These results are the consequence of the conductivity and permittivity properties of the tissues. In fact, muscle tissue has the highest conductivity and permittivity value followed by adipose tissue, followed by air.

Not so different are the results obtained from the difference of the 75th and 25th percentiles. In fact, it can be noted that the distance intervals between Tx and Rx obtained for the homogeneous model of air are of the same order of magnitude as those of the homogeneous model of muscle, which are the smallest. Slightly higher is the range of percentiles obtained for the homogeneous fat model. However, as previously stated, the largest ranges were obtained for Duke's heterogeneous model.

These results make it clear how the composition of the human body, made up of different tissues of different natures, influences the localization of WCE. In fact, both muscle tissue and fat tissue make it difficult to precisely identify the distance between Tx and Rx due to their conductivity and permittivity. Furthermore, even the air model which theoretically should provide more accurate results, is characterized by a non-negligible localization error.

Chapter 4

Limitations and future work

In this chapter, the limitations of the study and the future work that could be done to improve the localization error of the WCE are briefly discussed. It is important to recognize the limitations of the model used in order to accurately interpret the results and understand how actions can be taken to improve localization.

In particular, in this study, a parameter that has not been taken into consideration is the orientation of the WCE. In all the results obtained (except for the analysis of the electric field emitted by the Tx antenna), only the orientation of the capsule parallel to the vertical axis of the body was evaluated. The values obtained for the capsule parallel to the x or y-axis were not examined. It would be interesting to better understand whether or not this variable can influence the uncertainty in the localization.

Furthermore, homogeneous or fully heterogeneous models were considered in this study. Instead, it would be useful to understand how heterogeneous combinations of two or more tissues can influence the analyzed parameters and consequently the localization uncertainty.

Given the values obtained for this localization method based on EM wave transmission, it would be interesting to compare these results to other localization methods present in the literature. Indeed, for different homogeneous and heterogeneous models, one could implement different simulations based on other methods and compare the data obtained. This analysis would be important in order to be able to use in clinical practice the method that minimizes the localization error. In this regard, one could also combine the data obtained with other methodologies such as inertial unit measurements, visual imaging processing, machine learning, magnetic techniques or implementing the Kalman filter.

Chapter 5

Conclusion

In this master thesis, a travel model of the WCE through the GI tract has been implemented for the evaluation of the influence of various human body tissues on the localization. In particular, a numerical simulation in FDTD with the Sim4Life software has been realized. In order to achieve this goal, several elements have been modeled. Initially, the Tx and Rx antennas were simulated. As regards the Tx antenna, it has been implemented as a dipole antenna which radiates at 868 MHz, therefore in radio frequencies. The Rx has also been modeled as dipole antennas. 12 Rx were chosen and the simulation was conducted with a variable distance of the Rx from the body surface, particularly inside and outside the body. For the modeling of the human body, the Duke model was chosen which represents the adult male and is part of the ViP. With this model, four simulations were conducted. In fact, three homogeneous models of air, fat and muscle respectively, and a heterogeneous one formed by the complete Duke were used to understand the influence of various tissues on localization given their different properties in terms of conductivity and permittivity.

Subsequently, the data obtained from the simulations were extracted and an analysis was conducted. In fact, for each of the simulations performed, the electric field data and the distance between Tx and Rx along the entire GI tract were extracted. Furthermore, a hyperbolic interpolation of the data was performed and the R^2 -value was evaluated. Then, four significant points along the GI tract were chosen for the analysis. In these locations, for each model, the obtained values of electric field and distance between Tx and Rx were compared in terms of maximum, minimum, average, 25th and 75th percentile values. In this case, the position of the Rx with respect to the body surface was kept constant at 2 mm outside the body. Furthermore, the orientation of the capsule was maintained along the z direction, parallel to the vertical axis of the body. Regarding the homogeneous air model, although one would expect that there would be no variation along the GI tract in the amount of electric field and distance between Tx and Rx, minimal

variations were observed. For the different conductivity and permittivity values of the homogeneous fat model, the obtained electric field and distance values between Tx and Rx are different from the data obtained for the previous model. However, no substantial changes in the observed parameters were recorded between the various locations along the GI tract. The homogeneous muscle model, being characterized by higher permittivity and conductivity values among those analysed, led to the presence of significant variations of the parameters used along the GI tract. The point that is most different in this case is the one in the small bowel, characterized by higher electric field values. The Duke heterogeneous model is the most complex among those analysed. For this reason, the obtained values of electric field and distance between Tx and Rx for different locations within the GI tract are different from each other and also differ from the homogeneous models previously considered.

Moreover, the electric field and the distance between Tx and Rx and the previously described parameters were evaluated for different distances of Rx relative to the body surface for each of the four simulations performed. In this case, the point along the GI tract at the end of the esophagus was chosen. In addition, the orientation of the WCE was maintained along the z-axis, but the position of the Rx relative to the skin varied in accordance with the simulated locations both inside and outside the body. From the analysis of the results obtained, we can deduce that for the homogeneous air model the position of Rx does not substantially influence the distance values between Tx and Rx and the electric field. For the homogeneous fat model, a bigger difference was recorded in the electric field values relating to Rx positions with respect to the skin very internal to the body or very external (-80 mm and 80 mm). Similarly in the previous model analysed, different behaviour between internal and external Rx positions was recorded for the muscle model. Finally, regarding Duke's heterogeneous model, the calculated parameters of electric field and distance between Tx and Rx undergo important variations when different positions of Rx with respect to the body surface are considered.

Furthermore, a comparison of the different input power of the Tx antenna has been taken into consideration. This analysis was conducted using the electric field obtained at the point at the end of the esophagus with an Rx position of 2 mm external to the body surface and an orientation along the z-axis for each of the four simulations. The electric field values were divided by the square root of the real part of the input power of the Tx antenna. The input power value obtained for air is three orders of magnitude smaller than the others. Therefore, when the division of the electric field by the square root of this value is evaluated, the homogeneous model of air is the one with the highest electric field. Then follows the input power of the homogeneous model of fat, while that for the homogeneous model of muscle and the heterogeneous Duke model are very similar and higher than the others.

To understand how much the different tissues influence the localization of the WCE, XY sections of the propagation of the electric field near the Tx antenna were

evaluated for orientations along the x, y, and z axes. It has been observed that for the homogeneous model of air there is an almost constant decrease with concentric circles of the electric field in the three orientations. For the other three simulations (homogeneous models of fat and muscle, and heterogeneous Duke) the decrease of the electric field is not constant, but directional. Since the Duke heterogeneous model is the most complex in terms of conductivity and permittivity of the body, the electric field decrease model is the most heterogeneous and directional both in the area around the Tx antenna and in the farthest one.

Finally a localization analysis was carried out. For each of the simulations conducted, the results obtained in the different positions along the GI tract were combined. Subsequently, the data were fitted using a cumulative hyperbola for each model. Next, three distances between Tx and Rx were chosen and with the curve fitted three corresponding electric field values were found. A small range of electric field values was then chosen and the corresponding distances between Tx and Rx were evaluated. The data were then analyzed in terms of maximum and minimum distance between Tx and Rx and range between the 75th and 25th percentile. These ranges of distance values were then used to evaluate the localization error. It has been noted that the greatest error, as might have been expected, is that obtained for the Duke heterogeneous model. Next, the largest errors were recorded for the homogeneous model of muscle, then fat and finally air. However, if we evaluate the percentile ranges between the 75th and 25th, the greatest value is always that of the Duke heterogeneous model, followed however by the homogeneous one of fat and finally by those of muscle and air.

The results obtained and the parameters considered make it clear that the localization of the WCE and its uncertainty depend on the characteristics of the tissues of which the human body is composed. In fact, the wide uncertainty ranges of the distance between Tx and Rx obtained for the homogeneous models of muscle and fat make it difficult to localize the WCE. Moreover, also the air model which should have generated significantly lower errors, showed rather high localization uncertainty.

Appendix A

Simulation code

A.1 Definitions of the functions present inside the code

```
1 import sys, os, shutil
2 import numpy as np
3 from math import pi, cos, sin, sqrt
4 import s4l_v1.model as model
5 import s4l_v1.simulation.emfdd as ftd
6 import s4l_v1
7 import s4l_v1.analysis as analysis
8 import s4l_v1.analysis.viewers as viewers
9 import s4l_v1.document as document
10 import random
11 import s4l_v1.units as units
12 from s4l_v1.model import Vec3, Translation, Rotation, Transform
13 import XCoreModeling
14
15 thisfile = True
16
17 def rotx(rx, matform = True):
18     matrix = np.array([[1, 0, 0, 0], [0, cos(rx), -sin(rx), 0], [0, sin(rx),
19     cos(rx), 0], [0, 0, 0, 1]])
20     if matform:
21         return Mat3(Vec3(matrix[0, :3]), Vec3(matrix[1, :3]), Vec3(
22     matrix[2, :3]))
23     return matrix
24
25 def roty(ry):
26     return np.array([[cos(ry), 0, sin(ry), 0], [0, 1, 0, 0], [-sin(ry), 0, cos(
27     ry), 0], [0, 0, 0, 1]])
```

```

25
26 def rotz(rz):
27     return np.array([[cos(rz), -sin(rz), 0, 0], [sin(rz), cos(rz),
28     , 0, 0], [0, 0, 1, 0], [0, 0, 0, 1]])
29
30 def transl(tx, ty, tz):
31     return np.array([[1, 0, 0, tx], [0, 1, 0, ty], [0, 0, 1, tz], [0, 0, 0, 1]])
32
33 def openFile(pathfile):
34     try:
35         document.Open(pathfile)
36     except RuntimeError:
37         print('RuntimeError ignored')
38
39 def testandsetstartconf(antenna, basetransform):
40     for ent in antenna.Entities:
41         if not equaltransforms(ent.Transform, basetransform[ent.Name]):
42             ent.Transform = basetransform[ent.Name]
43
44 def equaltransforms(t, u):
45     m, n = t.Matrix4, u.Matrix4
46     all([m.Get(i, j) == n.Get(i, j) for j in range(4) for i in range(4)])
47     return all([(np.asarray(t.Scaling) == np.asarray(u.Scaling)).all(),
48     (np.asarray(t.Rotation) == np.asarray(u.Rotation)).all(), (np.asarray(t.Translation) == np.asarray(u.Translation)).all()])
49
50 def setTransform(group, targettransformdict):
51     for gi in group.Entities:
52         gi.Transform = targettransformdict[gi.Name]
53
54 def makealllocsduke11():
55     c01 = {'name': 'c01', 'transl': Translation(Vec3([143.0, 336.0, 1163.0]))}
56     c02 = {'name': 'c02', 'transl': Translation(Vec3([161.0, 271.0, 1032.0]))}
57     c03 = {'name': 'c03', 'transl': Translation(Vec3([96.0, 263.0, 980.0]))}
58     c04 = {'name': 'c04', 'transl': Translation(Vec3([141.0, 223.0, 1166.0]))}
59     c05 = {'name': 'c05', 'transl': Translation(Vec3([168.0, 278.0, 1080.0]))}
60     c06 = {'name': 'c06', 'transl': Translation(Vec3([153.0, 328.0, 1080.0]))}
61     c07 = {'name': 'c07', 'transl': Translation(Vec3([131.0, 347.0, 1096.0]))}

```

```

62     c08 = {'name': 'c08', 'transl': Translation(Vec3
63           ([158.0, 231.0, 1069.0]))}
64     c09 = {'name': 'c09', 'transl': Translation(Vec3
65           ([138.0, 267.0, 983.0]))}
66     c10 = {'name': 'c10', 'transl': Translation(Vec3
67           ([172.0, 278.0, 1111.0]))}
68     c11 = {'name': 'c11', 'transl': Translation(Vec3
69           ([161.0, 321.0, 1134.0]))}
70     return [c01, c02, c03, c04, c05, c06, c07, c08, c09, c10, c11]
71
72 def makeallocsdukegrid():
73     nx, ny, nz = 5, 5, 8
74     xrange = np.linspace(30, 180, nx, endpoint = True)
75     yrange = np.linspace(138, 398, ny, endpoint = True)
76     zrange = np.linspace(950, 1300, nz, endpoint = True)
77     allallocs = []
78     for i, xi in enumerate(xrange):
79         if i < 2 or i > 2:
80             continue
81         for j, yi in enumerate(yrange):
82             for k, zi in enumerate(zrange):
83                 name = 'c'+str(i)+str(j)+str(k)
84                 if int(name[1:]) != 224:
85                     continue
86                 if (i*j*k)%2 == -1:
87                     continue
88
89                 allallocs.append({'name': name, 'transl': Translation(Vec3
90                                   ([xi, yi, zi]))})
91     return allallocs
92
93 def makeallocsduke():
94     ninter = 10
95     truepos = 1000*np.array([[0.143, 0.264, 1.505],
96                               [0.125, 0.271, 1.474],
97                               [0.111, 0.27, 1.448],
98                               [0.096, 0.264, 1.415],
99                               [0.093, 0.26, 1.376],
100                              [0.09, 0.261, 1.339],
101                              [0.102, 0.275, 1.298],
102                              [0.131, 0.3, 1.265],
103                              [0.116, 0.322, 1.282],
104                              [0.115, 0.354, 1.293],
105                              [0.152, 0.343, 1.261],
106                              [0.16, 0.312, 1.237],
107                              [0.17, 0.286, 1.21],
108                              [0.168, 0.253, 1.194],

```

```
106 [0.163, 0.223, 1.198],
107 [0.133, 0.216, 1.19 ],
108 [0.139, 0.226, 1.16 ],
109 [0.17 , 0.263, 1.165],
110 [0.154, 0.294, 1.181],
111 [0.137, 0.317, 1.197],
112 [0.159, 0.351, 1.214],
113 [0.127, 0.347, 1.178],
114 [0.154, 0.334, 1.146],
115 [0.169, 0.299, 1.128],
116 [0.17 , 0.27 , 1.109],
117 [0.161, 0.24 , 1.096],
118 [0.156, 0.226, 1.067],
119 [0.168, 0.265, 1.073],
120 [0.161, 0.305, 1.094],
121 [0.128, 0.348, 1.111],
122 [0.15 , 0.335, 1.071],
123 [0.16 , 0.306, 1.056],
124 [0.159, 0.271, 1.041],
125 [0.152, 0.267, 1.01 ],
126 [0.137, 0.262, 0.987],
127 [0.105, 0.268, 0.976],
128 [0.069, 0.26 , 0.979],
129 [0.087, 0.233, 0.975],
130 [0.153, 0.24 , 0.969],
131 [0.158, 0.212, 0.996],
132 [0.156, 0.196, 1.023],
133 [0.143, 0.189, 1.053],
134 [0.127, 0.186, 1.084],
135 [0.118, 0.184, 1.118],
136 [0.119, 0.185, 1.148],
137 [0.16 , 0.21 , 1.158],
138 [0.16 , 0.225, 1.125],
139 [0.169, 0.257, 1.145],
140 [0.17 , 0.288, 1.168],
141 [0.169, 0.316, 1.194],
142 [0.158, 0.331, 1.215],
143 [0.128, 0.359, 1.24 ],
144 [0.119, 0.373, 1.206],
145 [0.107, 0.37 , 1.168],
146 [0.097, 0.368, 1.128],
147 [0.11 , 0.365, 1.092],
148 [0.121, 0.358, 1.059],
149 [0.145, 0.346, 1.021],
150 [0.158, 0.324, 0.996],
151 [0.157, 0.295, 1.005],
152 [0.148, 0.296, 0.981],
153 [0.146, 0.291, 0.956],
154 [0.113, 0.294, 0.947],
```

```

155         [0.082, 0.289, 0.949],
156         [0.048, 0.27 , 0.947],
157         [0.056, 0.259, 0.919],
158         [0.073, 0.26 , 0.893],
159         [0.071, 0.262, 0.857]])
160 nnew = (len(truepos)-1)*ninter+1
161
162 p0 = np.repeat(truepos, ninter, axis = 0)
163 dif = np.diff(truepos, axis = 0)
164 incr = np.einsum('i,jk->jik', np.linspace(0,1,ninter,endpoint =
False), dif).reshape((-1,3))
165 assert incr.shape[0] == nnew-1
166 truepos = p0[:nnew]
167 truepos[:nnew-1] = truepos[:nnew-1] + incr
168
169 alllocs = []
170 for i in range(nnew):
171     cnr = i//ninter
172     internr = i%ninter
173     cnrstring = f'{cnr:02d}'
174     internrstring = f'{internr:03d}'
175     name = 'c'+cnrstring+'cc'+internrstring
176     alllocs.append({'name':name, 'transl':Translation(Vec3([float(
ii) for ii in list(truepos[i]))]))})
177 return alllocs
178
179 def makealllocsfats():
180     truepos = np.load(r'D:\no backup\07 Localization\dipole\
alllocsfats.npy')
181     N = truepos.shape[0]
182     alllocs = []
183     for i in range(N):
184         name = 'c'+f'{i:03d}'
185         alllocs.append({'name':name, 'transl':Translation(Vec3([float(
ii) for ii in list(truepos[i]))]))})
186     return alllocs

```

A.2 Main code

```

1 rottox = Transform( Vec3(1, 1, 1), Vec3(0, 1.5708, 0), Vec3(0, 0, 0)
)
2 rottoy = Transform( Vec3(1, 1, 1), Vec3(-1.5708, 0,0), Vec3(0, 0, 0)
)
3 rottoz = Transform( Vec3(1, 1, 1), Vec3(0, 0,0), Vec3(0, 0, 0) )
4 rot1 = {'name': 'along X', 'rot':rottox}

```

```

5 rot2 = { 'name': 'along Y', 'rot': rottoy }
6 rot3 = { 'name': 'along Z', 'rot': rottoz }
7
8
9 basetransform = { 'Arm 1 - TX': Transform( Vec3(1, 1, 1), Vec3(0,0,0),
    Vec3(0, 0, 0) ), 'Lines 1 - TX': Transform( Vec3(1, 1, 1), Vec3
    (0,0,0), Vec3(0,0,0) ), 'Arm 2 - TX': Transform( Vec3(1, 1, 1),
    Vec3(0,0,0), Vec3(0,0,-4) ), 'Sphere 1 - TX': Transform( Vec3(1,
    1, 1), Vec3(0,0,0), Vec3(0,0,0) ) }
10
11
12 xrotvectors = [-1,0,1]
13 yrotvectors = [-1,0,1]
14 zrotvectors = [-1,0,1]
15 allrotvectors = [[xi,yi,zi] for xi in xrotvectors for yi in
    yrotvectors for zi in zrotvectors if xi+yi*10+zi*100 > 0]
16 allrotvectors = [[1,0,0],[0,1,0],[0,0,1]][:]
17
18 allrotdict = {}
19 for ri in allrotvectors:
20     name = 'R-x'+str(ri[0])+'-y'+str(ri[1])+'-z'+str(ri[2])
21     allrotdict[name] = ri
22
23 simnr = 1
24 simsuffix = r'sims '+str(int(simnr))+'\ '
25 startpath = r'D:\users\student\ '
26 alllocs = makealllocsduke()
27
28 startfile = 'start duke.smash'
29 savepath = startpath + simsuffix
30
31
32 try:
33     wicasim3 = s4l_v1.simulation.GetAvailableServers()['WICASIM3']
34 except:
35     print('wicasim 3 not found')
36 try:
37     wicasim4 = s4l_v1.simulation.GetAvailableServers()['WICASIM4']
38 except:
39     print('wicasim 4 not found')
40
41 count = 0
42 cxprevious = '-1'
43
44 document.Save()
45
46 for i,ci in enumerate(alllocs):
47     print('count: ',count)
48     cxnrstr = ci['name'][1:3]

```

```

49 if int(cxnrstr) != cxprevious:
50     openFile(startpath+startfile)
51     document.SaveAs(savepath+'conf c'+cxnrstr+'x.smash')
52 cxprevious = cxnrstr
53
54 print('Opened and saved')
55 try:
56     antenna = model.AllEntities()['Group 1']
57 except:
58     antenna = model.AllEntities()['TX']
59
60 for rname, roti in allrotdict.items():
61
62     confrotname = 'conf'+ci['name']+' - rot'+rname
63
64     print('start transform')
65     setTransform(antenna, basetransform)
66     testandsetstartconf(antenna, basetransform)
67
68     antenna.ApplyTransform(Rotation(Vec3([0,0,1]),Vec3(roti)))
69     antenna.ApplyTransform(ci['transl'])
70     a2 = antenna.Clone()
71     a2.Name = a2.Name + ci['name'] + rname
72     for a2i in a2.Entities:
73         a2i.Name = a2i.Name + ci['name'] + rname
74
75     print('Start sim')
76
77     simstart = document.AllSimulations['EM S01']
78     sim = simstart.Clone()
79     sim.Name = 'EM'+ci['name'] + rname
80     confrotname = 'conf'+ci['name']+' - rot'+rname
81     document.AllSimulations.Add(sim)
82
83     print('Startsave')
84
85     document.Save()
86
87     print('Start grid')
88     sim.GlobalGridSettings.TopPadding = sim.GlobalGridSettings.
TopPadding + np.array([0,0,max(0,ci['transl'].Translation
[2]-1400+50)])
89     if ci['name'][:3] in ['c67','c68']:
90         sim.GlobalGridSettings.BottomPadding = sim.
GlobalGridSettings.BottomPadding + np.array([0,0,50])
91
92     sim.UpdateGrid()
93     print('Start voxeling')
94     sim.CreateVoxels()

```

```
95     print('Voxels created')
96     document.Save()
97     print('Start run')
98     sim.RunSimulation(server_id = wicasim4, wait = True)
99     document.Save()
100     count += 1
101
102 print('Ready')
```

Appendix B

Data conversion code

B.1 From smash data to npy data

```
1 allcons = makealllocsduke()
2
3 xrotvectors = [-1,0,1][:1]
4 yrotvectors = [-1,0,1][:1]
5 zrotvectors = [-1,0,1][2:]
6 allrotvectors = [[xi,yi,zi] for xi in xrotvectors for yi in
7     yrotvectors for zi in zrotvectors if xi+10*yi +100*zi > 0]
8 allrotvectors = [[1,0,0],[0,1,0],[0,0,1]][-1:]
9
10 allrotdict = {}
11 for ri in allrotvectors:
12     name = 'R-x'+str(ri[0])+'-y'+str(ri[1])+'-z'+str(ri[2])
13     allrotdict[name] = ri
14
15 count = 0
16 sensors = []
17 quantities = []
18 quantities = ["EM E(x,y,z,f0)"]
19
20 if thisfileonly:
21     if not fromimport:
22         simlist = list(s4l_v1.document.AllSimulations)[1:]
23     else:
24         import importlib
25         import s4l_analysis_fromimport
26         importlib.reload(s4l_analysis_fromimport)
27         s4l_analysis = s4l_analysis_fromimport
28         from s4l_analysis import *
```

```

28     simlist = [sim for sim in document.AllAlgorithms if sim.Name
29 [-10:] == '(imported)']
30     for sim in simlist:
31         simname = sim.Name
32         print(simname)
33         confrotfilename = 'conf ' +simname[simname.find('c'):simname.
34 find('R')] + ' - rot R-' + simname[simname.find('R')+2:]
35         if confrotfilename[-11:] == '(imported)':
36             confrotfilename = confrotfilename[:-11]
37             if os.path.isfile(os.path.join(exportpath, confrotfilename+'.
38 npy')):
39                 pass
40                 continue
41             results = {}
42             results = getFieldSensorData(sim, results, sensors,
43 quantities)
44             np.save(os.path.join(exportpath, confrotfilename+'.npy'),
45 results)
46             print('Saved np: ',str(os.path.join(exportpath,
47 confrotfilename+'.npy')))
48 else:
49     for ci in allcons:
50         print('ci:',ci)
51         conffilename = 'conf '+ci['name']
52         smashpath = startpath+confilename + ".smash"
53         openFile(smashpath)
54         for sim in list(s4l_v1.document.AllSimulations)[1:]:
55             print('sim:',sim.Name)
56             confrotfilename = 'conf ' +ci['name'] + ' - rot R-' + sim.
57 Name[sim.Name.find('R')+2:]
58             results = {}
59             results = getFieldSensorData(sim, results, sensors,
60 quantities)
61             np.save(os.path.join(exportpath, confrotfilename+'.npy'),
62 results)
63             print('Saved np: ',str(os.path.join(exportpath,
64 confrotfilename+'.npy')))
65             document.Save()
66 print('Ready2')

```

B.2 Extract electric fields

```

1 rxcopath = r 'C:\Users \... \ duke\ \ '
2

```

```

3 fieldupperpath = r'D:\users\...\\'
4 fieldpath = fieldupperpath + r'exports e\'
5
6 dvalues = [2,4,6,8,10,14,20,30,50,80]
7 dvalues = [-d for d in dvalues] + dvalues
8
9 nrzpoints = 41
10 nrthetapoints = 63
11
12
13 reload = True
14 eonly = True
15
16 c01 = {'name': 'c01'}
17 c02 = {'name': 'c02'}
18 c03 = {'name': 'c03'}
19 c04 = {'name': 'c04'}
20 c05 = {'name': 'c05'}
21 c06 = {'name': 'c06'}
22 c07 = {'name': 'c07'}
23 c08 = {'name': 'c08'}
24 c09 = {'name': 'c09'}
25 c10 = {'name': 'c10'}
26 c11 = {'name': 'c11'}
27 rot1 = {'name': 'along X'}
28 rot2 = {'name': 'along Y'}
29 rot3 = {'name': 'along Z'}
30
31
32
33 xrotvectors = [-1,0,1]
34 yrotvectors = [-1,0,1]
35 zrotvectors = [-1,0,1]
36 allrotvectors = [[xi,yi,zi] for xi in xrotvectors for yi in
37     yrotvectors for zi in zrotvectors if xi + 10*yi + 100*zi >0]
38 allrotvectors = [[1,0,0],[0,1,0],[0,0,1]][:]
39
40 allrotdict = {}
41 allrotnames = []
42
43 allrots = []
44 for ri in allrotvectors:
45     name = 'R-x' + str(ri[0]) + '_y' + str(ri[1]) + '_z' + str(ri[2])
46     allrots.append({'name':name, 'vector':ri})
47
48 virtualradius = 0.15
49
50 allcons = [c01, c02, c03, c04, c05, c06, c07, c08, c09 ,c10, c11][:]

```

```

51 nrcons = len(allcons)
52 nrrots = len(allrots)
53 notfoundlist = []
54
55 of = 'Overall Field'
56 e = 'EM E(x,y,z,f0)'
57 h = 'EM H(x,y,z,f0)'
58 s = 'S(x,y,z,f0)'
59
60 count = 0
61
62
63 for file in os.listdir(fieldpath)[::1]:
64     print(file)
65     for tt in range(1):
66
67         if count < -1:
68             count += 1
69             continue
70
71         if file[-4:] != '.npy':
72             count += 1
73             continue
74         confrotfilename = file[:-4]
75         confrotfilenamepickle = confrotfilename + '_pickle'
76
77         picklepathtest = fieldupperpath + r'pickle 2D fields\\' + r'd'
78         + str(dvalues[0]) + ' +' + '{0:.2f}'.format(
79             virtualradius) + r'\\'
80         if os.path.isfile(picklepathtest + confrotfilenamepickle + '.pkl
81         '):
82             print('skipped')
83             continue
84
85         try:
86             print(fieldpath + confrotfilename + '.npy')
87             alldata = np.load(fieldpath + confrotfilename + '.npy',
88             allow_pickle=True).item()
89         except FileNotFoundError:
90             print('Field file not found, skipped')
91             print('\t', fieldpath + confrotfilename)
92             notfoundlist.append(confrotfilename)
93             count += 1
94             continue
95
96     print('stopload')
97
98     try:
99         E = alldata[list(alldata.keys())[0]][of]['E']

```

```

97     except:
98         print('J')
99         raise()
100
101     ex = E['x']
102     ey = E['y']
103     ez = E['z']
104     ee = E['E']
105     ex, ey, ez = [(ei[:-1] + ei[1:])/2 for ei in [ex, ey, ez]]
106     if not eonly:
107         hh = alldata[list(alldata.keys())[0]][of]['H']['H']
108         ss = alldata[list(alldata.keys())[0]][of]['S']['S']
109
110     if np.max(np.isnan(ee)):
111         print('nan value found in e field')
112         print(f'file: {file}')
113         raise()
114
115     e3d = np.swapaxes(ee.reshape((len(ez) , len(ey) , len(ex) , 3)
116 ), 0, 2)
117     if not eonly:
118         h3d = np.swapaxes(hh.reshape((len(ez) - 1, len(ey) - 1,
119 len(ex) - 1, 3)), 0, 2)
120         s3d = np.swapaxes(ss.reshape((len(ez) - 1, len(ey) - 1,
121 len(ex) - 1, 3)), 0, 2)
122
123     for di in dvalues:
124         skipflag = False
125         ucofile = 'skinco00_d' + str(di) + '.npz'
126         print(ucofile)
127
128         picklepath = fieldupperpath + r'pickle 2D fields\\' + r'd
129 ' + str(di) + ' '+'{0:.2f}'.format(virtualradius) \
130         +r'\\'
131         uco = np.load(rxcopath + ucofile)
132
133         nrofcols = 13 if not eonly else 7
134         ucoindsfieldsall = np.zeros((uco.shape[0], nrofcols)).
135 astype(complex)
136
137         for i, ucoi in enumerate(uco[:]):
138             xi, yi, zi = np.argmax(ex > ucoi[0]), np.argmax(ey >
139 ucoi[1]), np.argmax(ez > ucoi[2])
140             if ex[-1] < ucoi[0] or ey[-1] < ucoi[1] or ez[-1] < ucoi
141 [2]:
142                 xi = len(ex) - 1 if ex[-1] < ucoi[0] else xi
143                 yi = len(ey) - 1 if ey[-1] < ucoi[1] else yi
144                 zi = len(ez) - 1 if ez[-1] < ucoi[2] else zi
145             if not eonly:

```

```

139         ucoindsfieldsall[i] = [ex[xi], ey[yi], ez[zi],
ucoi[3] ] + list(e3d[xi, yi, zi,
140                 :])+ list(h3d[xi, yi, zi, :])+ list(s3d[xi, yi, zi
, :])
141         else:
142             ucoindsfieldsall[i] = [ex[xi], ey[yi], ez[zi],
ucoi[3] ] + list(e3d[xi, yi, zi, :])
143             if skipflag:
144                 print('d skin (not) skipped, because at domain
boundary; d = ', di )
145                 finterpolall = NearestNDInterpolator(list(zip(
ucoindsfieldsall[:, 2], ucoindsfieldsall[:,
146                     3]*virtualradius)), ucoindsfieldsall[:, 0:
nrofcols])
147                 print('interpol done')
148                 znew = np.linspace(0.95, 1.3, nrzpoints)
149                 tnew = np.linspace(-3.1, 3.1, nrthetapoints)*
virtualradius
150                 tnew = np.linspace(-3.14, 3.14, nrthetapoints)*
virtualradius
151
152                 znewgrid, tnewgrid = np.meshgrid(znew, tnew)
153                 enewall = finterpolall(znewgrid, tnewgrid)
154                 if np.max(np.isnan(enewall)):
155                     raise ValueError('nan found in interpolated fields')
156                 enewalltransp = np.moveaxis(enewall, 1, 0)
157
158                 t_z_enewallt = (tnew, znew, enewalltransp)
159                 if not os.path.exists(picklepath):
160                     os.makedirs(picklepath)
161                 with open(picklepath + confrotfilenamepickle+'.pkl', 'wb'
) as fi:
162                     pickle.dump(t_z_enewallt, fi)
163                     count += 1
164
165 print('Readyyyy')
```

Bibliography

- [1] F.H. Martini, M.J. Timmons, and R.B. Tallitsch. *Anatomia Umana*. EdiSES, 2019 (cit. on p. 1).
- [2] J. Gordon Betts et al. *Anatomy and Physiology*. OpenStax College, Rice University, Houston, Texas, 2013 (cit. on p. 2).
- [3] F. Bianchi, A. Masaracchia, E. Shojaei Barjuei, A. Menciacchi, A. Arezzo, A. Koulaouzidis and D. Stoyanov, P. Dario, and G. Ciuti. «Localization strategies for robotic endoscopic capsules: a review». In: *Diagnostics* 2022 12 (2022), pp. 381–403 (cit. on pp. 2, 7, 8).
- [4] D. R. Kohli and J. Baillie. *Clinical Gastrointestinal Endoscopy*. Elsevier, 2019 (cit. on pp. 3, 4).
- [5] Boese A. et al. «Endoscopic Imaging Technology Today». In: *Expert Review of Medical Devices* 16 (2019) (cit. on p. 3).
- [6] K. Taniguchi et al. *Robot surgery*. InTech. doi:10.5772/6893, 2010 (cit. on p. 3).
- [7] J. Kovaleva. «Endoscope drying and its pitfalls». In: *Journal of Hospital Infection* (2017) (cit. on p. 3).
- [8] P. Rogalski, J. Daniluk, A. Baniukiewicz, E. Wroblewski, and Andrzej Dabrowski. «Endoscopic management of gastrointestinal perforations, leaks and fistulas». In: *World Journal of Gastroenterology* (2015) (cit. on p. 4).
- [9] Swain C., Gong F., and Mills T. «Wireless transmission of a colour television moving image from the stomach using a miniature CCD camera». In: *Nature* 405 (1999) (cit. on p. 4).
- [10] Seung-Joo Nam et al. «3D reconstruction of small bowel lesions using stereo camera-based capsule endoscopy». In: *Nature* (2020) (cit. on p. 5).
- [11] Y. Guo and G. Shao. «Wireless Localization for a Capsule Endoscopy: Techniques and Solutions». In: *Antenna and Sensor Technologies in Modern Medical Applications* (2021), pp. 191–234 (cit. on pp. 6, 10).

- [12] A.C. Ormeci et al. «Retention during capsule endoscopy: Is it a real problem in routine practice?» In: *Journal of International Medical Research* 44 (2016), pp. 968–975 (cit. on p. 6).
- [13] A. K. H. Chong, B. W. K. Chin, and C. G Meredith. «Clinically significant small-bowel pathology identified by double-balloon enteroscopy but missed by capsule endoscopy». In: *Gastrointestinal Endoscopy* (2006), pp. 445–449 (cit. on p. 6).
- [14] Z. Fireman, D. Paz, and Y. Kopelman. «Capsule endoscopy: improving transit time and image view». In: *World Journal of Gastroenterology: WJG* (2005) (cit. on p. 6).
- [15] M. F. Hale, R. Sidhu, and M. E. McAlindon. «Capsule endoscopy: Current practice and future directions». In: *World J. Gastroenterol* 20.24 (2014), pp. 7752–7759 (cit. on p. 6).
- [16] P. S. Boroujeni, H. N. Pishkenari, H. Moradi, and G. Vossoughi. «Model-aided real-time localization and parameter identification of a magnetic endoscopic capsule using extended Kalman filter». In: *IEEE Sensors Journal* 21 (June 2021), pp. 13667–13675 (cit. on p. 7).
- [17] M. F. Hale, R. Sidhu, and M. E. McAlindon. «A Video-based Speed Estimation Technique for Localizing the Wireless Capsule Endoscope inside Gastrointestinal Tract». In: *36th Annual International Conference of the IEEE Engineering in Medicine and Biology Society (EMBC)* 123 (2014) (cit. on p. 7).
- [18] N.Marya, A.Karellas, A.Foley, A.Roychowdhury, and D.Cav. «Computerized 3-dimensional localization of a video capsule in the abdominal cavity: Validation by digital radiography». In: *Gastrointestinal Endoscopy* 79.4 (2014), pp. 669–674 (cit. on p. 7).
- [19] A. M. Franz, T. Haidegger, W. Birkfellner, K. Cleary, T. M. Peters, and L. Maier-Hein. «Electromagnetic Tracking in Medicine — A Review of Technology, Validation, and Applications». In: *IEEE Transaction in medical imaging* 33 (Aug. 2014), pp. 1702–1725 (cit. on p. 7).
- [20] U. Khan, Y. Ye, A.-U-Aisha, P. Swar, and K. Pahlavan. «Precision of EM Simulation Based Wireless Location Estimation in Multi-Sensor Capsule Endoscopy». In: *IEEE Journal of Translational Engineering in Health and Medicine* 6 (2018), pp. 2168–2372 (cit. on p. 7).
- [21] A. M. Franz, T. Haidegger, W. Birkfellner, K. Cleary, T. M. Peters, and Lena Maier-Hein. «Electromagnetic Tracking in Medicine—A Review of Technology, Validation, and Applications». In: *IEEE Transactions on Medical Imaging* 33.8 (2014), pp. 1702–1725 (cit. on p. 7).

- [22] H. Mateen, Md. R. Basar, A. U. Ahmed, and M. Y. Ahmad. «Localization of Wireless Capsule Endoscope: A Systematic Review». In: *IEEE Sensors Journal* 17.11 (2017), pp. 1197–1206 (cit. on p. 8).
- [23] A. Koulaouzidis et al. «Novel experimental and software methods for image reconstruction and localization in capsule endoscopy». In: *Endoscopy International Open* (2018), pp. 205–210 (cit. on p. 8).
- [24] A. R. Nafchi, S. T. Goh, and S. A. Reza Zekavat. «Circular Arrays and Inertial Measurement Unit for DOA/TOA/TDOA-Based Endoscopy Capsule Localization: Performance and Complexity Investigation». In: *IEEE Sensors Journal* 14.11 (2014), pp. 3791–3799 (cit. on p. 9).
- [25] A. Wille, M. Broll, and S. Winter. «Phase difference based RFID navigation for medical applications». In: *2011 IEEE International Conference on RFID* (2011) (cit. on p. 9).
- [26] Y. Ye, K. Pahlavan, G. Bao, P. Swar, and K. Ghaboosi. «Comparative Performance Evaluation of RF Localization for Wireless Capsule Endoscopy Applications». In: *International Journal of Wireless Information Networks volume 8* (2014), pp. 208–222 (cit. on p. 10).
- [27] M. Barbi, C. Garcia-Pardo, A. Nevárez, V. Pons Beltrán, and N. Cardona. «UWB RSS-Based Localization for Capsule Endoscopy Using a Multilayer Phantom and In Vivo Measurements». In: *IEEE Transactions on antennas and propagation* 67.8 (Aug. 2019), pp. 5035–5043 (cit. on pp. 10, 11).
- [28] J. Goethals, A.M. Leys, G. Vermeeren, M. Deruyck, L. Martens, and W. Joseph. «Dog IoT: Path Loss and Link Budget Analysis for Canine Wireless Body Area Network». In: *2022 16th European conference on antennas and propagation (EUCAP)* (2022) (cit. on p. 14).
- [29] M.-C. Gosselin et al. «Development of a new generation of high-resolution anatomical models for medical device evaluation: the Virtual Population 3.0». In: *Institute of Physics and Engineering in Medicine* 59 (2014), pp. 5287–5303 (cit. on pp. 17, 18).
- [30] H.-P. Müller, F. Raudies, A. Unrath, H. Neumann, A. C. Ludolph, and J. Kassubek. «Quantification of human body fat tissue percentage by MRI». In: *NMR in Biomedicine* 24 (2011) (cit. on p. 19).